ISBN 978-82-471-2528-1 (printed ver.)
ISBN 978-82-471-2529-8 (electronic ver.)
ISSN 1503-8181

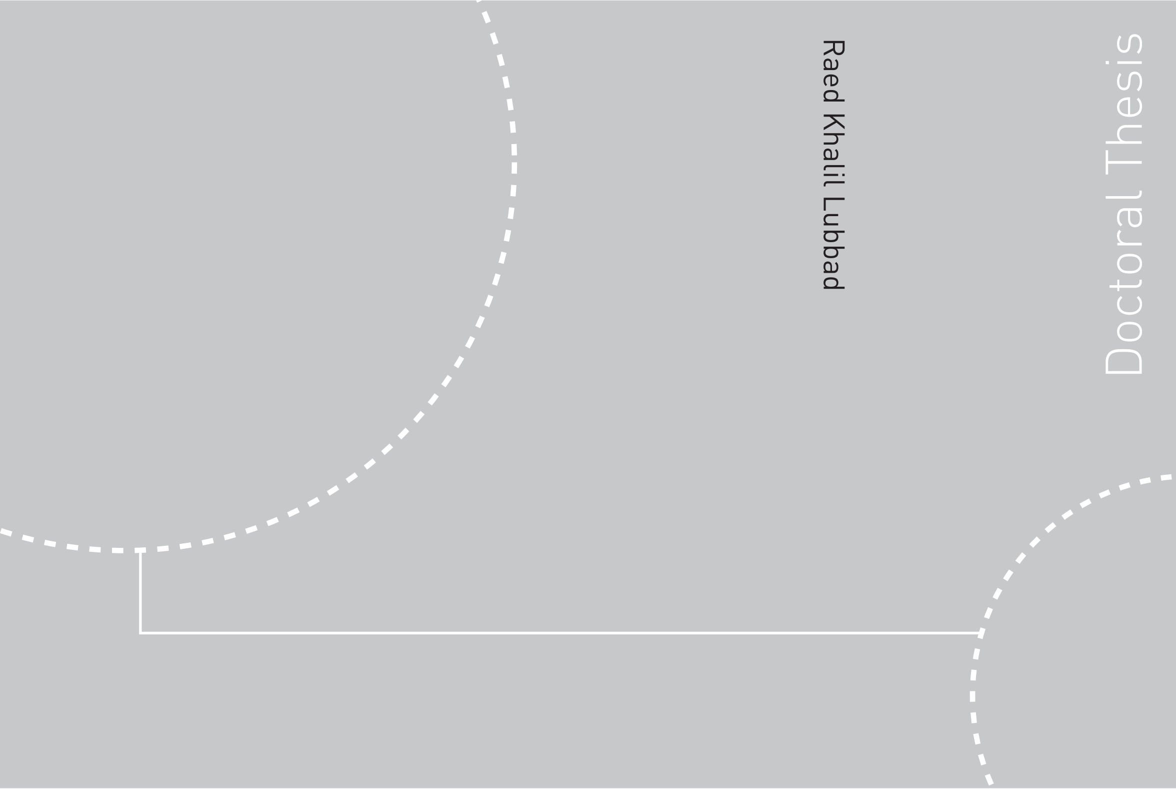

Raed Khalil Lubbad

Doctoral Thesis

Doctoral theses at NTNU, 2011:9

**NTNU**
Norwegian University of
Science and Technology
Thesis for the degree of
philosophiae doctor
Faculty of Engineering Science and Technology
Department of Civil and Transport Engineering

Doctoral theses at NTNU, 2011:9

Raed Khalil Lubbad

# Some Aspects of Arctic Offshore Floating Structures

NTNU
Norwegian University of
Science and Technology

Raed Khalil Lubbad

# Some Aspects of Arctic Offshore Floating Structures

Thesis for the degree of philosophiae doctor

Trondheim, January 2011

Norwegian University of
Science and Technology
Faculty of Engineering Science and Technology
Department of Civil and Transport Engineering

NTNU
Norwegian University of
Science and Technology

**NTNU**
Norwegian University of Science and Technology

Thesis for the degree of philosophiae doctor

Faculty of Engineering Science and Technology
Department of Civil and Transport Engineering

©Raed Khalil Lubbad

ISBN 978-82-471-2528-1 (printed ver.)
ISBN 978-82-471-2529-8 (electronic ver.)
ISSN 1503-8181

Doctoral Theses at NTNU, 2011:9

Printed by Tapir Uttrykk

To my parents

## ABSTRACT

The present work highlights some aspects related to the analyses of Arctic offshore floating structures. This thesis consists of five papers, which can be divided into two main categories. One category deals with the dynamics of slender structures with an emphasis on the prediction and suppression of vortex induced vibrations (VIV), and the other category examines the process of interaction between sloping structures and sea ice with focus on developing a numerical model to simulate this process in real time.

Slender structures, such as mooring lines and marine risers, are very important for the offshore petroleum industry, which is currently approaching deeper waters. Increasingly, attention has been focused on predicting the susceptibility of these structures to VIV. In this thesis, two asymptotic techniques namely, the local analysis and the WKB methods, were used to derive closed-form solutions for the natural frequencies and mode shapes of slender line-like structures. Both the top-tensioned nearly-vertical configuration and the catenary configuration were considered. The accuracy of the solutions derived was established through comparison with other analytic solution techniques and with results of numerical finite element solutions. The effects of the bending stiffness and the effects of approximating the tension variation as a linear function were discussed. Experimental data on the multi-modal in-line and cross-flow response behaviour of a towed catenary model were analysed to examine the usefulness of the solutions for predicting the response frequencies and envelopes due to VIV.

Helical strakes are often used as a mitigating measure to suppress the VIV of slender structures. This thesis presented an innovative method to fit ropes helically to a riser in the installation phase. Such a procedure will help to overcome the handling problem associated with the use of conventional sharp-edged strakes. Experimental investigations were then performed to verify the efficiency of these ropes (round-sectioned helical strakes) in suppressing VIV. Systematic experimental investigations including twenty-eight configurations of round-sectioned helical strakes were tested in an attempt to find the most suitable strake configuration. The effects of varying pitch, the surface roughness and the ratio between the cross-flow and in-line natural frequencies on the efficiency of the proposed configuration of round-sectioned helical strakes were also investigated.

The process of interaction between sea ice and offshore sloping structures (e.g., conical structures and ship-shaped structures) is quite complex. Modelling this process is very demanding and often computationally expensive, which typically hinders the chances for real-time simulations. This kind of simulation can be very useful for training personnel for Arctic offshore operations and procedures, for analysing the efficiency of various ice management concepts and as a part of the onboard support systems for station keeping. The challenge of meeting the real-time criterion was overcome in the present work. This thesis developed a numerical model to simulate the process of interaction between sea ice and sloping structures in real time. In this model, only level- and broken-ice features were studied. New analytical closed-form solutions were established and used to represent the ice breaking process. *PhysX* was used for the first time to solve the equations of rigid body motions with six degrees of freedom for all ice floes in the calculation domain. The results of the simulator were validated against experimental data from model-scale and full-scale tests.

Accurate predictions of ice actions are also vital to optimise the design of the structures in the Arctic regions. A good understanding of the role of seawater in the process of interaction between the sloping structures and level ice will help to establish reliable models to estimate the ice forces. This work formulated both the static and dynamic bending problems for a floating wedge-shaped ice beam interacting with an offshore sloping structure. For the dynamic interaction, the effects of the water foundation on the bending failure of the ice were studied by comparing the results of an elastohydrodynamic approach with a model of a Winkler foundation. The thesis also investigated the breaking lengths of the ice wedges (i.e., the frequency of the ice loads) as a function of the ice thickness, the compression in the ice and the acceleration of the interaction.

## ACKNOWLEDGEMENTS

As I go through my work for the past few years, I often find my mind wandering through many pleasant memories involving many people who became personal icons and beloved friends. It is to them that I owe my success in completing this important chapter of my life.

My hearty appreciation goes to my mentor and supervisor, Professor Sveinung Løset, who believed in me and in my ability to serve the science I chose as my discipline. It is to this great scientist that I owe my knowledge and my designation. Professor Sveinung Løset's positive influence on my life extends beyond the borders of academia to the folds of my personal life. Thanks indeed, Sveinung, for your continuous support and generosity, which have always inspired me.

I am thankful to my co-supervisor Professor Geir Moe for the valuable discussions and encouragement throughout the past years. His kind support and instructive supervision have been of tremendous importance in adding to my knowledge and experience.

Many thanks to Professor Ove Tobias Gudmestad for his interest in my projects and the imprints he left through his encouraging and constructive discussions. I am also thankful to Professors Alf Tørum, Knut Villhelm Høyland and Øivind Arntsen for their help and support throughout my PhD studies.

I have been fortunate to have had the opportunity to meet and work with Professor John Niedzwecki, who invited me to stay and work at Texas A&M University for a few months. I am grateful for his hospitality and cooperation. Many thanks go to Dr. Tuomo Kärnä for involving me in his experiment at Hamburg Ship Model Basin (HSVA) and to the ice tank crew at HSVA for their hospitality as well as technical and scientific support.

My deep appreciation goes to the Faculty of Engineering Science and Technology at the Norwegian University of Science and Technology (NTNU) for funding my PhD programme. I am thankful to Statoil for funding the experimental work at the Harbour and Coastal Laboratories at NTNU. I would like to thank the Research Council of Norway, Statoil, Det Norske Veritas and the Ship Manoeuvring Centre (SMS) for the financial support for the real-time simulation project. Here, I would also like to thank the Norwegian coast guard for their hospitality and cooperation onboard the *KV Svalbard.*

My deep appreciation is due to my parents who have been very supportive, loving and encouraging throughout my many years of studies. I am thankful to my family in Palestine and Canada for their never-ending love and support. I would like to thank my dear friends in Norway for all the good times. My appreciation is also owed to Jørgen, Kristen and Helga Varden for their hospitality, support and love throughout my years in Trondheim.

I would like to thank Mr. Ole Jacob Hagen and Mr. Stig Rune Søberg from SMS for their help and cooperation in building and validating the real-time simulator. Additionally, I thank Mr. Adimas Pribadi for helping me perform part of the experimental work presented in this thesis. I would like to thank the technician Gustav Jakobsen for facilitating my experimental work at the Harbour and Coastal Laboratories at NTNU.

I use this opportunity to praise the unique environment at the "PhD basement", where I was always surrounded by colleagues who were happy to cooperate, discuss, and exchange ideas. We have had memorable times with a lot of fun activities. I thank everyone who contributed to this special atmosphere in the basement. Thank you Kenneth Eik, Felix Breitschädel, Nicolas Serre, Vegard Aksnes, Oddgeir Dalane, Ada Repetto-Llamazares, Lucie Strub-Klein,

Christian Lønøy, Haiyan Long, Marit Reiso, Daniel Zwick, Eric Van Buren, Karl Merz, Kim Yangkyun, Fengwei Guo, Johan Wåhlin, Wolfgang Kampel, Sergiy Sukhorukov, Anton Kulyakthin, Wenjun Lu, Ivan Metrikin and Ekaterina Kim. Additionally, I would like to thank Drs. Arne Gürtner, Simon-Philippe Breton, Pavel Liferov, Basile Bonnemaire, Morten Bjerkås, Jens Laugesen, Jenny Trumar, Alex Klein-Paste and Paul Thomassen. A big "thank you" also goes to our administrators Marion Beentjes and Elin Tønset for their care and great help.

# TABLE OF CONTENTS

ABSTRACT ........................................................................................................i

ACKNOWLEDGEMENTS ...................................................................................iii

TABLE OF CONTENTS .....................................................................................v

**1.** INTRODUCTION.........................................................................................1

**2.** ASPECTS OF ARCTIC OFFSHORE FIELD DEVELOPMENT..................................7

**3.** CLOSED-FORM SOLUTIONS FOR VIBRATIONS OF NEARLY VERTICAL STRINGS AND BEAMS BY MEANS OF ASYMPTOTIC METHODS .................. 25

**4.** FREQUENCY AND MODE SHAPE ESTIMATES OF MARINE CATENARY SYSTEMS USING ASYMPTOTIC APPROXIMATIONS .......................................... 35

**5.** EXPERIMENTAL INVESTIGATIONS OF THE EFFICIENCY OF ROUND-SECTIONED HELICAL STRAKES IN SUPPRESSING VORTEX INDUCED VIBRATIONS ........................................................................................ 61

**6.** A NUMERICAL MODEL FOR REAL-TIME SIMULATION OF SHIP-ICE INTERACTION ........................................................................................ 73

**7.** STATIC AND DYNAMIC INTERACTION OF FLOATING WEDGE-SHAPED ICE BEAMS AND SLOPING STRUCTURES ..................................................... 93

**8.** SUMMARY, CONCLUSIONS AND RECOMMENDATIONS FOR FURTHER WORK ............................................................................................... 107

# CHAPTER 1

# INTRODUCTION

## Contents

**1. INTRODUCTION** .......... **3**

**1.1 Objective, Scope and Organisation of the Thesis** .......... **4**

**1.2 Readership** .......... **6**

# 1 INTRODUCTION

This thesis considers different aspects of floating structures in Arctic waters. Vortex-induced vibrations (VIV) as well as ice actions on floaters are discussed.

Cost-effective and thus slender structures are essential for the offshore petroleum industry. One example of these structures is mooring lines and spread mooring systems, which are commonly used to provide station keeping for buoys, barges, ships and floating offshore platforms. Another example is marine risers, which are used for the drilling of subsea wells, for well intervention and also for the flow of well fluids to production facilities at the sea surface.

The dynamic performance of these long, slender, line-like structures is very important for the structural safety and thus must be analysed carefully. Potential hazards may include:

a) Dynamic amplification of the structural response when the frequency of the external excitation is near one of the natural frequencies of the slender structure. A safe design must ensure that the available margin to accommodate the dynamic tension is sufficient.

b) Flow-induced vibrations (e.g., VIV, galloping, flow interference, buffeting, static divergence, and drag crisis). The effects of these vibrations on the tension variation, on the fatigue life of the structure and on the hydrodynamic forces must be considered.

c) Impact forces due to, e.g., a collision between two risers in a bundle of risers or an ice block hitting a riser. The structural response to these forces must be considered.

Marine slender structures are often modelled as tension dominated cables or beams due to their line topology and the applied pretension. The dynamics of these models are complicated by non-linearities that may be due to the geometry, material properties, hydrodynamic forces, effects of structural interaction with the sea bed, or some combination of these factors. Mathematically, it is possible to formulate a set of nonlinear coupled partial differential equations to serve as the basis for the dynamic analyses of these structures. Depending upon the complexity of the model, numerical solutions may require a substantial computational time and depending on the numerical model they may only provide global quantitative response results and consequently little understanding of the relative influences of the various parameters that govern the problem solution.

An alternative formulation that utilises asymptotic methods can be used to derive analytical approximations for the natural frequencies and corresponding mode shapes of a slender structure. As a consequence of initially assuming that the dynamic response is relatively small, the undamped cable or beam formulations lead to distinct natural frequencies and mode shapes that depend only on the static configuration and the boundary conditions. The closed-form solutions for the eigenvalue problem can be useful in several ways: 1) they enhance the understanding of how the different structural parameters affect the structural response to the external loadings; 2) they simplify the modal analysis of the structural response; 3) based upon these approximate solutions, one can assess whether excitation from the environment is sufficiently near any natural frequencies of the structure that the response could be amplified in the damping controlled region, potentially leading to the undesirable acceleration of fatigue or other design problems; or, in other words, 4) they can be used for practical problems to assess whether higher order approximations or more complex analyses are needed to more adequately address relevant system nonlinearities.

In this thesis, two asymptotic techniques were used, namely, the local analysis and the WKB methods, to derive closed-form solutions for the natural frequencies and mode shape of marine slender structures. Both the top-tensioned nearly-vertical configuration and the catenary configuration were studied. The usefulness of the derived analytical solutions was emphasised in predicting the VIV of marine risers and mooring lines.

VIV is a major design concern. These vibrations increase the drag forces acting on slender structures and may cause fatigue damage. Therefore, it is of the utmost importance to accurately predict such vibrations and to have dependable methods by which to suppress them when necessary. Helical strakes are commonly used as a mitigating measure to suppress VIV. The edge of these strakes causes flow separation to occur at the strake, and the helical shape disturbs the axial correlation of the vortices, which reduces the global lift force. Helical strakes are simple, reliable and omni-directional. Their use involves some disadvantages, however, mostly related to handling problems during the installation and amplification of the drag coefficient when the riser is not vibrating. In this thesis, an innovative method to fit ropes helically to a riser in the installation phase is discussed. This procedure will help to overcome the handling problems associated with the use of conventional helical strakes. Then, experimental data to verify the efficiency of these ropes (round-sectioned helical strakes) in suppressing VIV are presented.

The expansion of the petroleum industry towards the Arctic offshore presents new challenges. The search for hydrocarbons in the deep Arctic waters requires the use of drillships and floating production units (FPUs). Typically, these units require protection by using ice management. In particular, the ship-shaped FPUs must implement ice vaning to avoid excessive loads in the pack ice. Each of these activities requires site-specific operations, with icebreakers battling large ice floes, followed by icebreakers downstream that cut the ice into small pieces just in front of the drillship or FPU. To operate effectively, an assessment of the operations is essential, and here real-time simulators have great potential in a number of applications. These simulators, if calibrated and validated properly, can be a useful tool for training the crews for Arctic operations and procedures. Real-time simulators can also be used to analyse the efficiency of various ice management concepts, and, in the future, such simulators may even be part of the onboard support systems for station keeping. In this thesis, a numerical model was developed to simulate in real time the process of interaction between ice and ships (or conical structures). In this model, only level- and broken-ice features were studied. The results of the real-time simulator model were validated against experimental data from model-scale and full-scale tests.

Accurate predictions of ice actions are also vital to optimise the design of structures in the Arctic regions. A good understanding of the ice-water-structure interaction process will help to establish reliable models to estimate the ice forces. In this thesis, the dynamic bending problem of a floating wedge-shaped ice beam interacting with a sloping structure was studied. Here, the fully-coupled elastohydrodynamic approach was compared with the model of a Winkler foundation to study the effects of seawater on the interaction process. Finally, the breaking lengths (i.e., the frequency of the ice actions) were studied as a function of the ice drift acceleration, the ice thickness and the in-plane compression in the ice.

## 1.1 Objective, Scope and Organisation of the Thesis

This thesis highlights some aspects of the slender structure dynamics, which are very important for the offshore petroleum industry. The thesis also touches upon some of the new challenges that face the offshore industry in the Arctic regions. The objectives of the present study can be summarised as follows:

- To develop analytical closed-form solutions for the natural frequencies and the mode shapes of slender offshore structures. Both the top-tensioned nearly-vertical configuration and the catenary configuration are considered.

- To predict the characteristics of VIV of slender structures using the derived closed-form solutions for the natural frequencies and mode shapes.

- To study the efficiency of round-sectioned helical strakes in suppressing VIV.

- To develop a reliable model for the calculations of ice actions on offshore structures (e.g., conical structures and ship-shaped structures). Both level ice and broken ice features are considered.

- To develop a numerical model for real-time simulations of ship-ice interactions.

- To study the effects of seawater on the dynamic interaction between level ice and offshore structures.

The thesis consists of five papers, which I wrote together with my supervisors. For each of these papers, I was the first author and conducted the major part of the work. The papers can be divided into two main categories: 1) dynamics of slender offshore structures with an emphasis on VIV prediction and suppression and 2) ice actions on offshore structures with a focus on developing a numerical model to simulate the process of interaction in real time. Each paper is given a chapter number, and the thesis is organised as follows:

**Chapter 2** discusses aspects of Arctic offshore field developments. It introduces different types of offshore structures and argues that the floating structures are most suitable for the Arctic offshore. Some design challenges of the Arctic floaters are then highlighted, which include VIV and the estimation of ice actions, which are the main focus of this thesis.

**Chapter 3** describes the derivations of analytical closed-form solutions for vibrations of nearly-vertical strings and beams by means of asymptotic methods. Derivations are shown in reasonable detail. The chapter presents a simple example in which the bottom tension in a marine riser is only 9% of the top tension. The example is analysed for cases with and without bending stiffness, and the solutions are compared to the exact solution for the string case and to the results from three finite element programs for the beam case.

**Chapter 4** shows the derivations of closed-form approximate solutions of the cross-flow natural frequencies and mode shapes for a catenary. The accuracy of these approximations is established through comparison with other analytic solution techniques and with results from numerical finite element solutions. The effects of the bending stiffness and the effects of approximating the tension variation along the catenary as a linear function are discussed. Additionally, the paper presents experimental data on the multi-modal, in-line and cross-flow response behaviour of a towed catenary model. Such data provide a means to illustrate the usefulness of the analytical asymptotic approximations derived for predicting the response frequencies and envelopes due to the VIV.

**Chapter 5** presents experimental investigations of the efficiency of round-sectioned helical strakes in suppressing VIV. Systematic experimental investigations including twenty-eight configurations of round-sectioned helical strakes were tested in an attempt to find the most suitable strake configuration. The paper studies the effects of varying the strake pitch, the effects of surface roughness and the effects of the ratio between the cross-flow and in-line natural frequencies on the efficiency of the proposed configuration of round-sectioned helical strakes.

**Chapter 6** develops a numerical model for the real-time simulation of ship-ice interactions. New analytical closed-form solutions are established and used to represent the ice breaking process. *PhysX* is used for the first time to solve the equations of rigid body motions for six degrees of freedom for all ice floes in the calculation domain. The results of the numerical model are validated against experimental data from model-scale and full-scale tests.

**Chapter 7** formulates both the static and dynamic problems for a floating wedge-shaped ice beam interacting with an offshore sloping structure. For the dynamic interaction, the effects of seawater are studied by comparing the results of the elastohydrodynamic approach with the model of a Winkler foundation. The paper also investigates the breaking lengths of the ice wedges (i.e., the frequency of the ice loads) as a function of the ice thickness, the compression in the ice and the acceleration of the interaction.

**Chapter 8** summarises the main conclusions from the present study and discusses some recommendations for further work.

## 1.2 Readership

The present work focuses on offshore structures needed for the exploration and production of hydrocarbons. Attention has been given to the dynamics of slender structures and to the environmental actions from level and broken ice features. The primary readership for this thesis is students, engineers, lecturers and scientists working with the following:

- The dynamic analysis of slender line-like structures.
- The problems of flow-induced vibrations in general and VIV in particular.
- The design of offshore structures in ice-infested waters.
- The development of hydrocarbon fields in the Arctic offshore, especially tasks related to ice management and station keeping.

# CHAPTER 2

# ASPECTS OF ARCTIC OFFSHORE FIELD DEVELOPMENT

# Contents

2. ASPECTS OF ARCTIC OFFSHORE FIELD DEVELOPMENT ....................................9

- 2.1 Offshore Structures ....................................9

- 2.2 Arctic Floaters .................................... 10

- 2.3 Vortex Induced Vibrations .................................... 12
  - 2.3.1 Relevant Nondimensional Parameters .................................... 13
  - 2.3.2 Prediction of VIV .................................... 15
  - 2.3.3 Suppression of VIV .................................... 16
    - 2.3.3.1 Increase reduced damping .................................... 16
    - 2.3.3.2 Avoid resonance .................................... 16
    - 2.3.3.3 Streamline cross section .................................... 16
    - 2.3.3.4 Add a vortex suppression device .................................... 17

- 2.4 Ice Actions .................................... 17
  - 2.4.1 Ice Action Parameters .................................... 18
  - 2.4.2 Dynamic Ice Actions .................................... 19
  - 2.4.3 Level Ice Action on Sloping Structures .................................... 20

- References .................................... 23

# 2 ASPECTS OF ARCTIC OFFSHORE FIELD DEVELOPMENT

The increase in demand for oil and gas as well as the paucity of new giant onshore discoveries are pushing the petroleum industry to explore and develop offshore fields in deepwater and ultra deepwater basins, i.e., commonly defined with minimum bathymetric depths of 400 m and 1500 m, respectively. Moreover, the huge hydrocarbons reserves in the Arctic and the shrinking of the Arctic ice cover due to global warming are also encouraging oil companies to expand their offshore activities to the Arctic.

## 2.1 Offshore Structures

The development of an offshore hydrocarbon field requires the deployment of offshore structures to perform the drilling, production, storage, offloading, intervention, and other logistic operations. Figure 2.1 shows different types of offshore structures used by the petroleum industry. These structures can generally be divided into the following three categories:

- Fixed structures, e.g., gravity-based structures, jackets and compliant towers.
- Floating structures, e.g., semi-submersibles, floating production units, drill ships, tension-legs, and spars.
- Subsea arrangements that are tied back to host facilities.

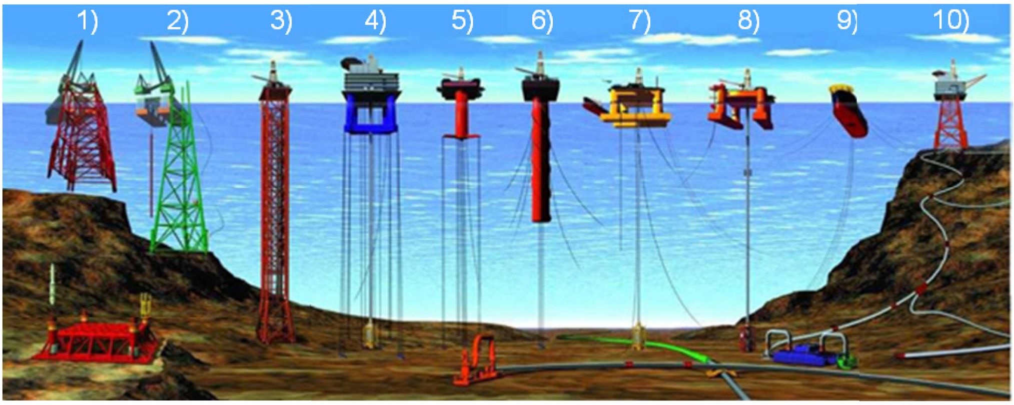

Figure 2.1: Types of offshore oil and gas structures include 1, 2) conventional fixed platforms (deepest at 412 m); 3) compliant towers (deepest at 534 m); 4, 5) vertically moored tension leg and mini-tension leg platforms (deepest at 1425 m); 6) spars (deepest at 1710 m); 7,8) semi-submersibles (deepest at 1920 m); 9) floating production, storage, and offloading facilities (deepest at 1345 m); and 10) sub-sea completion and tie-back to host facilities (deepest at 2307 m). *All records from 2005 data* (Ocean Explorer [1]).

The economical feasibility of fixed structures is questionable for deepwater projects. Fully subsea developments are currently not attractive for remote offshore fields where the distance to shore is roughly more than 150 km. The Snøhvit (145 km from shore) and Ormen Lange (120 km from shore) are examples of cutting edge subsea projects. Floating structures are the most suitable for the development of offshore hydrocarbon fields, especially those fields located in deepwater and remote locations. Many of the potential future oil and gas provinces are indeed in deepwater locations, and they are remote and often also prone to ice; see Annex B in the ISO Code [2]. Another advantage of the use of floaters in the Arctic offshore is that they may be disconnectable and thus capable of moving away to avoid impacts with, e.g., icebergs.

## 2.2 Arctic Floaters

A floating system can include 1) a hull, 2) marine systems, 3) accommodation, 4) hydrocarbon processing facilities, 5) storage, 6) offloading systems, 7) station-keeping system, i.e., mooring or dynamic positioning, 8) umbilical connections, and 9) risers to connect the hull with the well head at the seabed.

An Arctic floater can be classified based on its shape, mobility and function. As indicated in Figure 2.2, the floater may have a hull form that is either ship-shaped or non-ship-shaped. The non-ship-shaped floaters can further be classified as column stabilised, self-elevating, deep draught and tension leg floaters; see DNVOSS-102 [3]. The ship-shaped floaters can act as free-going vessels, and they also have the possibility of maintaining a geofixed position by the use of a mooring or a dynamic positioning (DP) system. Free-going vessels provide support and a means of transportation both for personnel and hydrocarbons. It is worth mentioning here that ship transportation by tankers is inherently more flexible than pipeline transportation and is also cheaper for long distances. Icebreakers are often used to apply physical ice management in ice-covered waters. Floaters that apply station-keeping by means of mooring or DP systems are useful for the drilling, production, storage, offloading, service and intervention operations. The latter is typically performed from floaters on DP.

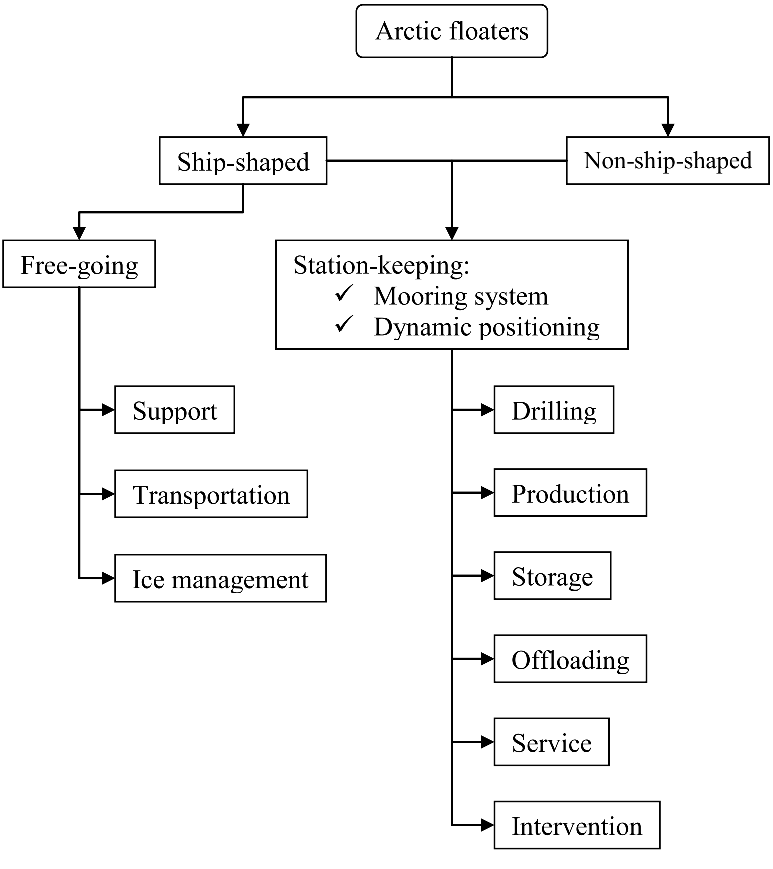
Arctic floaters
Ship-shaped
Non-ship-shaped
Free-going
Station-keeping:
✓ Mooring system
✓ Dynamic positioning
Support
Transportation
Ice management
Drilling
Production
Storage
Offloading
Service
Intervention

Figure 2.2: Classification of floaters based on their shape, mobility and function.

Figure 2.3 shows a sketch of different types of floaters used in the development of the Terra Nova field on the Grand Banks. Both ship-shaped and non-ship-shaped floaters are utilised on that field. The sea ice conditions are not severe on the Grand Banks, but icebergs may intrude into the area occasionally. Therefore, the floating production storage offloading unit (FPSO) was designed with disconnection capabilities. Other examples of Arctic offshore floaters can be found in Gudmestad et al. [4].

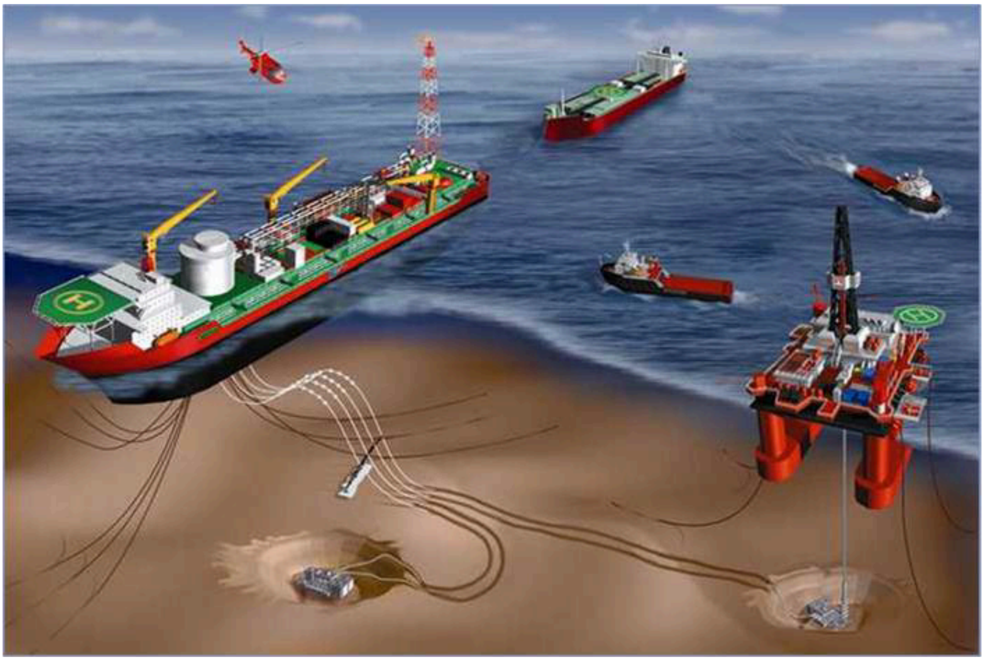

Figure 2.3: Different types of floaters used in the development of the Terra Nova field on the Grand Banks, Lever et al. [5].

The structural design of a floating system requires, e.g., a careful analysis of the environmental actions, the response of every component in the system and the coupling between the different components. The structure must be designed for the actions of wind, waves, currents, ice and perhaps seismic activities. A typical loading scenario in ice-covered waters is a combined action from drifting ice and ocean currents. For instance, waves are heavily attenuated by sea ice, and, thus, for intact level ice and highly concentrated broken ice, wave and ice loads are not likely to appear simultaneously (Frankenstein et al. [6]). The ice forces act mainly on the hull; however, in certain circumstances, ice blocks may also impact the submerged slender components, e.g., mooring lines and risers. The response of the hull to the ice actions will modify the characteristics of the risers and mooring lines and, in return, influence the level of the ice forces exerted on the hull. The response of risers and mooring lines to ocean currents adjusts the stiffness and damping of the floating system. The current-induced vibrations of some floaters and to larger extent the vibrations of the submerged slender parts can jeopardise the safety of the whole concept. The dynamic behaviour of the submerged slender parts is also very important during and after any disconnection operation, and it may be very decisive for the degree of success of such operations.

This thesis contributes to the complex picture above in the following ways:

1. By studying the vortex-induced vibrations (VIV) of slender line-like structures, e.g., risers and umbilical and mooring lines.
2. By studying the actions of level and broken ice features on a floating hull.

Analytical closed-form solutions are derived for the natural frequencies and mode shapes of slender structures. These solutions are then suggested as practical engineering tools to examine the susceptibility of slender structures to VIV. The solutions derived are also useful for the empirical models, which predict the VIV behaviour by assuming that the structural response will occur at a single or a discrete number of frequencies. Moreover, this thesis introduces an innovative method to install round-sectioned helical strakes, and it verifies the efficiency of these strakes in suppressing VIV. Finally, a numerical model is developed to simulate in real time the interaction between a floater and sea ice, and a closer look is directed towards the effect of the seawater on such interactions.

## 2.3 Vortex Induced Vibrations

The vibrations caused by vortex shedding have potentially destructive effects on structures, which can be manifested as, e.g., fatigue damage and the amplification of the in-line drag forces. Hence, it is essential to take into consideration these vibrations whilst designing offshore structures, especially slender structures such as marine risers and mooring lines.

To illustrate the process of vortex shedding, we can apply Bernoulli's equation to the potential flow around a circular cylinder. Then, it follows that the pressure reaches its maximum value at the front stagnation point where the velocity is zero, and that the pressure is a minimum when the velocity attains its maximum value at 90º. Furthermore, the pressure is expected to increase again towards the aft stagnation point. This causes the fluid particles that exist near the cylinder surface to use their kinetic energy to travel against the increasing pressure. In the meantime, those particles in viscid fluid lose a portion of their energy due to the friction forces, and, therefore, they are no longer capable of following the potential flow streamline that could reach the aft stagnation point. At last, as a result of the pressure gradient, the flow near the cylinder surface reverses and causes the boundary layer to separate from each side of the cylinder, which ultimately forms two shear layers that trail towards the rear of the cylinder. The point at which the separation occurs is called the separation point. The innermost part of the separated shear layer that is still in contact with the cylinder, moves slower than the outermost part, which makes contact with the free stream. This is why the shear layers roll into the near wake and fold on each other, forming the vortices. These vortices grow and finally separate from the cylinder and travel downstream.

Because the vortex shedding alternates from one side of the cylinder to the other, the pressure around the cylinder becomes periodically fluctuating. This fluctuation in the pressure generates time variable forces both in the in-line and the cross-flow directions. The frequency of the lift forces (cross-flow forces) is the same as the vortex shedding frequency, whereas the frequency of the in-line forces is twice the shedding frequency. Finally, when the vortex shedding frequency reaches the natural frequency of the cylinder, the cylinder is likely to be excited to oscillate. Here, it is essential to watch carefully how the vibrations are maintained over a range of flow velocities. In this range, the frequency of vortex shedding remains locked onto the natural frequency of the oscillating cylinder, which is known as the lock-in range, where the cylinder motion controls the process of vortex shedding. The lock-in phenomenon is simply a process of fluid-structure interaction. On one side, the motion of the cylinder affects the flow and changes its behaviour, whereas, on the other side, the flow may change the vibration frequency of the cylinder.

The complexity of the VIV process comes from the modification of the flow pattern around the structure as a function of a number of factors, including the Reynolds number, which will be defined later, the turbulence level, the surface roughness, three-dimensionality, and the flow-structure interaction. The flow field around stationary or oscillating cylinders and the effects of the abovementioned factors are not discussed here. Discussions of this subject can be found in Zdravkovich [7, 8], Blevins [9] and Chakrabarti [10].

The following section provides an introduction to the most important nondimensional parameters, which are frequently used in studying VIV. Section 2.3.2 briefly discusses different approaches for the prediction of VIV of marine risers and cables. Finally, Section 2.3.3 reviews the available methods that are used to suppress VIV.

### 2.3.1 Relevant Nondimensional Parameters

The nondimensional parameters that are often used to study VIV can be divided into three groups: flow, structural, and fluid-structure interaction parameters. According to Blevins [9], the aspect ratio, reduced velocity, dimensionless amplitude, mass ratio, Reynolds number, damping factor and turbulence intensity are the most useful parameters in describing the vibration of an elastic structure in steady flow. These parameters and a few others are defined below.

#### Reynolds number ($\boldsymbol{Re}$)

The Reynolds number describes the ratio between inertia forces and viscous forces in the boundary layer. It is written as

$$Re = \frac{UD}{\nu} \tag{2.1}$$

where $U$ is the flow velocity, $D$ is the diameter of the cylinder, and $\nu$ is the kinematic viscosity.

#### Turbulence intensity

The turbulence intensity is a measure of the fluctuations in the mean flow and is defined by the relation

$$\frac{u_{rms}}{U} \tag{2.2}$$

where $u_{rms}$ is the root mean square turbulence and $U$ is the free-stream velocity.

#### Aspect ratio

The aspect ratio of a cylinder gives information about its geometrical shape and is defined as

$$\frac{L}{D} \tag{2.3}$$

where $L$ is the length and $D$ is the diameter of the cylinder.

#### Roughness ratio

The roughness ratio describes the conditions of the body surface and is defined as

$$\frac{k}{D} \tag{2.4}$$

where $k$ is the characteristic size of the roughness and $D$ is the diameter of the cylinder.

**Mass ratio**

The mass ratio is the ratio between the mass per unit length of the cylinder $(m)$ and the mass per unit length of the displaced fluid $(\pi\rho D^2/4)$, multiplied by $\pi/4$. The mass ratio is written as

$$\frac{m}{\rho D^2} \tag{2.5}$$

where $\rho$ is the density of the fluid. The added mass is included by some authors in the mass per unit length, but other authors exclude this added mass and consider only the structural mass.

**Specific gravity**

The specific gravity is the ratio between the mass per unit length of the cylinder $(m)$ and the mass per unit length of the displaced fluid $(\pi\rho D^2/4)$, which gives

$$\frac{4m}{\pi\rho D^2} \tag{2.6}$$

The specific gravity is approximately 1.27 times the mass ratio.

**Damping ratio $(\zeta_n)$**

The damping ratio describes the structural damping and is defined as

$$\zeta_n = \frac{c_n}{2m_n\omega_n} \tag{2.7}$$

where $\omega_n$ is the $n^{\text{th}}$ natural frequency in radians per second, $c_n$ is linear damping coefficient in the $n^{\text{th}}$ mode and $m_n$ is the mass that corresponds to $\omega_n$ and the actual restoring force $k_n$.

**Reduced velocity $(U_r)$**

The reduced velocity is a useful parameter when presenting the structural response in the lock-in range. $U_r$ is the ratio of the path length travelled in one cycle in the flow direction and the cylinder diameter. It can be defined as

$$U_r = \frac{UT}{D} = \frac{U}{fD} \tag{2.8}$$

where $U$ is the flow velocity, $T$ is the oscillation period, $f$ is the frequency of oscillation in Hz and $D$ is the cylinder diameter. For tests that uses an elastically mounted cylinder, the cylinder's natural frequency, whether in air or in still water, is often used instead of the oscillation frequency.

**Nominal reduced velocity**

This parameter is the reduced velocity using the natural frequency in air.

**True reduced velocity**

This parameter is the reduced velocity using the true vibration frequency.

**Non-dimensional frequency**

This parameter is the inverse of the true reduced velocity.

**Dimensionless response amplitude**

The dimensionless response amplitude is the ratio between the vibration amplitude and the cylinder diameter:

$$\frac{A_x}{D} \; or \; \frac{A_y}{D} \tag{2.9}$$

where $A_x$ and $A_y$ are the vibration amplitudes in the in-line and cross-flow directions, respectively.

**Strouhal number $(S_t)$**

The Strouhal number is the proportionality constant of the relationship between the vortex shedding frequency and the flow velocity divided by the cylinder diameter. This number is written as

$$S_t = \frac{f_s D}{U} \tag{2.10}$$

where $f_s$ is the vortex shedding frequency, $U$ is the flow velocity and $D$ is the cylinder's diameter.

**Reduced damping $(K_s)$**

The reduced damping is very often used to predict the VIV response of structures. It has been used in many versions, and it can be found under many names, such as mass damping, Scruton number, or (combined) stability parameter. A common definition of the reduced damping is

$$K_s = \frac{2m\delta}{\rho D^2} \tag{2.11}$$

where $m$ is the cylinder mass per unit length and $\delta = 2\pi\zeta$ is the logarithmic decrement.

### 2.3.2 Prediction of VIV

This section discusses briefly the different methods available for the prediction of VIV of slender line-like structures. In principle, any of these methods would require solutions for the fluid forces as well as the structural response. The different approaches to solve this coupled system can be divided into the following three groups:

- Computational fluid dynamics (CFD) methods.
- Pragmatic methods.
- Empirical methods.

The CFD models work in the time domain, and they implement different numerical techniques to compute the flow around the structure. These models are generally based on solving the Navier-Stokes equations for the fluid and the beam equation for the slender structure simultaneously. The CFD models can be two-dimensional (2D) or three-dimensional (3D). The 2D models utilise the strip theory. They calculate the 2D flow around the structure on a large number of parallel planes distributed over the length of the beam. These planes communicate through the motion of the structure. The position of the structure is updated at each time step in response to the computed instantaneous flow-induced forces. The 3D models are more complex, and they are limited to a lower Reynolds number than the 2D models (Chakrabarti [10]).

The pragmatic methods are quite similar to the two-dimensional CFD models. The only difference here is that the solution of Navier-Stokes equations is not required because the fluid behaviour is idealised by simpler models, e.g., the wake oscillator model (see [9]).

The empirical models make no attempt to describe the flow field, and they are generally based on the assumption that VIV occurs at a single frequency or at discrete frequencies. Then, these models variously use experimental data to identify the amplitudes of the excited modes. The empirical models can be solved in the frequency domain and the time domain (see [11]).

### 2.3.3 Suppression of VIV

There are different approaches that are used to suppress the VIV. Blevins [9] stated that, by modifying either the structure or the flow, it is possible to reduce the amplitude of vibration and the related magnification of the steady drag. Furthermore, he divided the suppression options into four categories:

- Increase reduced damping
- Avoid resonance
- Streamline cross section
- Add a vortex suppression device

#### 2.3.3.1 Increase reduced damping

It is possible to increase the reduced damping $(K_S)$ by increasing the structural mass and/or the structural damping. According to Blevins [9], the peak amplitudes at resonance are less than 1% of the cylinder's diameter when $K_S > 64$.

#### 2.3.3.2 Avoid resonance

Resonance can be avoided if the frequency of vortex shedding is kept lower than the natural frequency of the riser, which may be achieved by stiffening the structure, especially if the structure is small.

#### 2.3.3.3 Streamline cross section

Streamlining the downstream side of the structure minimises the flow separation. Accordingly, the vortex shedding and the drag forces are considerably decreased. Blevins [9] stated that an effective streamlining requires a taper with an angle that is less than $8^o$ to $10^o$. Streamlined fairing or other trailing edges can be used for this purpose. The main drawback of this method is its directionality, which makes it suitable only for cases where the flow direction is fixed relative to the structure. The structure must also have sufficient stiffness to avoid flutter.

#### 2.3.3.4 Add a vortex suppression device

Different types of vortex suppression devices are available. Zdravkovic [12] classified those devices into three categories according to their mechanism of vortex suppression. Jones and Lamb [13] repeated to a great extent the same classification as follows:

- Topographic devices (Zdravkovic: Surface protrusions)
- Shrouds
- Wake devices (Zdravkovic: Nearwake stabilisers)

**Topographic devices**

A topographic device modifies the surface of the cylinder without being located predominantly in the wake of the cylinder. Topographic devices reduce the VIV by interfering with the boundary layer separation and, hence, disturbing the initiation and formation of the vortices. Topographic devices can be omnidirectional or unidirectional. Examples of topographic devices are helical strakes, wires, fins, studs and spheres.

**Shrouds**

The shroud is a device placed at a certain distance from the cylinder to allow the fluid to flow in between the shroud and the cylinder. This arrangement suppresses the VIV by affecting the three stages of the vortex shedding process (vortex initiation, formation, and shedding). The shroud can be many shapes, such as perforated, gauze, axial rods, and axial slats. Full shrouds are omnidirectional, and partial shrouds are unidirectional.

**Wake devices**

Wake devices lie predominantly in the wake of the cylinder. They reduce the VIV by interfering with vortex shedding and the last part of vortex formation. These devices are generally unidirectional and available in different styles (e.g., splitter and saw-tooth plates, guiding plates and vans).

### 2.4 Ice Actions

Assessment of ice actions is essential to optimise the design of offshore structures in the Arctic. The actions exerted by ice on the structures are usually divided into two types of actions, i.e., global and local. The global action is the sum of all action components on the whole structure at any instant time. For instance, it is quite common to characterise global ice actions on a vertical structure by effective (average) pressure acting over a nominal contact area (the product of the ice thickness and the structure width). Within the nominal contact area, however, there can be many spots subjected to higher pressure than the effective pressure. The local ice action is then defined as the local pressure applied on a limited part of the contact area, typically up to 2 $m^2$; see Løset et al. [14]. The estimation of the local ice action is useful for the evaluation of the local strength and is needed for the design of, e.g., shell or stiffening elements. The determination of global ice actions is necessary to 1) study the overall stability of structures, 2) design the foundations of fixed-structures, 3) analyse the capacity and behaviour of the station keeping systems of floating structures and 4) optimise the design and operation of free-going vessels in ice covered waters.

Based on the structural and ice properties, the actions of ice (both global and local) can be considered as static, quasi-static, cyclic or dynamic. The cyclic and dynamic actions may cause fatigue damage, foundation liquefaction and personnel discomfort. Moreover, rubble may accumulate around the structure in a manner that hinders the operations. All these factors must be considered whilst designing offshore structures for the Arctic.

A typical design of Arctic offshore structures will incorporate sloping surfaces at the waterline, e.g., conical structures, wide sloping structures and ship-shaped floaters. The conical structures (upward and downward sloping) are omnidirectional, meaning that the ice will always interact with a sloping surface regardless of the drifting direction. Ship-shaped floaters conversely are unidirectional, and ice vaning is usually required for the ice to interact with the sloping surfaces at the bow area. The main benefit of the sloping surfaces is that they promote the bending failure in ice over the other modes of failure, which helps to reduce the global ice actions. Sloping structures are also favoured because they are less susceptible than vertical structures to ice-induced vibrations. Nevertheless, the interaction between ice and sloping surfaces is a function of many variables, and it includes several processes, which together determine the global ice action.

A brief discussion of the main factors that govern the ice actions on structures is given in the following section. The dynamic ice actions are discussed in Section 2.4.2. Finally, attention is paid to the interaction between sloping surfaces and level ice (both intact level ice and broken ice), where the different processes are highlighted and their contributions to the global ice action are discussed.

### 2.4.1 Ice Action Parameters

There are many factors that govern the severity of ice actions on structures. The structural characteristics, the ice properties, and the physical environmental conditions may result in a number of interaction scenarios and may cause the ice to fail with different modes of failure, which will eventually determine the ice action; see Figure 2.4.

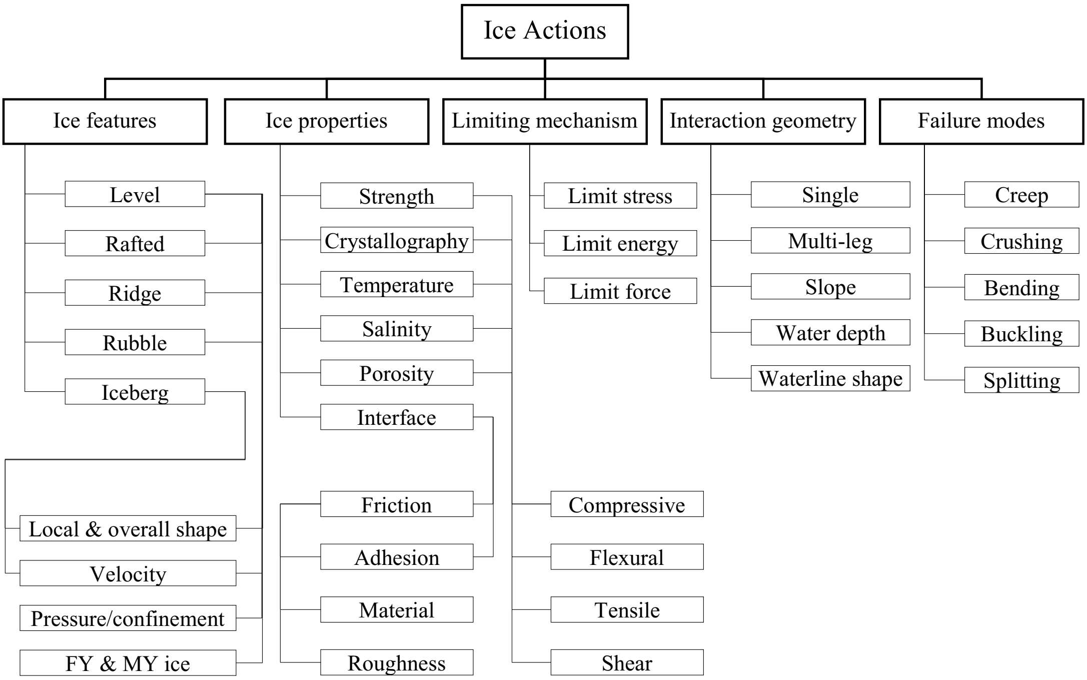
Ice Actions
Ice features
Ice properties
Limiting mechanism
Interaction geometry
Failure modes
Level
Rafted
Ridge
Rubble
Iceberg
Local & overall shape
Velocity
Pressure/confinement
FY & MY ice
Strength
Crystallography
Temperature
Salinity
Porosity
Interface
Friction
Adhesion
Material
Roughness
Limit stress
Limit energy
Limit force
Compressive
Flexural
Tensile
Shear
Single
Multi-leg
Slope
Water depth
Waterline shape
Creep
Crushing
Bending
Buckling
Splitting

Figure 2.4: Main factors governing the ice actions (figure reproduced from the ISO Code [2]).

Offshore structures in the Arctic are exposed to different types of ice features, e.g., intact level ice, broken ice fields, rafted ice, ridges, rubble fields and icebergs. The shape of the ice feature, the relative velocity between the ice and the structure, the confinement pressure in the ice and whether the ice is first-year or multi-year will have substantial influence on the interaction scenario. The spatial and temporal variation of ice properties is also very important for the determination of ice actions.

When an ice feature impacts a structure, the upper limit of the ice action will be bound by one of three limiting mechanisms: limit stress, limit energy or limit force. The mass of the ice feature, the initial impact velocity, the ice feature properties, the environmental driving forces and the structure shape and size will decide which one of these mechanisms is activated, as explained below.

**Limit stress**

The internal stresses in the ice increase as the contact force between the ice feature and the structure increases. If the stress in the ice exceeds a certain stress level, the ice feature will fail, and the contact forces will drop. Hence, the ice actions (contact forces) are limited by the internal stress and the ice strength. When the ice feature interacts with a vertical structure, the crushing failure mode will most likely dominate, and, therefore, the ice compressive strength will set the upper limit of the ice actions. On the other hand, the flexural strength of the ice will control the ice actions on the sloping structure because the dominating mode of failure in that case is most likely bending failure. In certain circumstances, other modes of failure are also possible, e.g., shear, creep, buckling, and splitting.

**Limit energy**

This interaction scenario arises when the kinetic energy of the ice feature is insufficient for enveloping the structure. In other words, the ice feature will stop shortly after impacting the structure. In the case of broken ice with relatively low concentration and if the structure is narrow, the ice feature will most likely travel around the structure. In this case, the actions related to the limit energy are generally less than those corresponding to the limit stress scenario.

**Limit force**

This scenario occurs if the ice feature stops shortly after impacting the structure and cannot be cleared away due to the large width of the structure and/or high concentration of the ice around it. Then, this halted ice feature start transmitting actions to the structure exerted by the wind, current and surrounding ice features. If these driving forces are sufficiently large, they may cause the structure to start penetrating again into the ice, which is usually associated with a slow interaction velocity and strong ice, leading to considerable ice actions. In the case that the surrounding ice is weaker than the ice feature adjacent to the structure, rafting and ridging will occur at the back of the halted ice feature.

### 2.4.2 Dynamic Ice Actions

Offshore structures may be exposed to two types of dynamic ice actions:

- Impact loading arising due to an impact with, e.g., an iceberg.
- Quasi-continuous loading resulting from the interaction with level ice.

According to the ISO [2], quasi-continuous ice loadings on offshore structures can be divided into three primary modes of interaction as follows:

- **Intermittent ice crushing.** It may occur if a compliant offshore structure is interacting with level ice at low speeds. This type of interaction is quasi-static, i.e., the maximum response of the structure coincides with the peak ice force, and transient decaying vibrations typically occur right after the peak ice force.
- **Frequency lock-in**. It may happen at intermediate interaction speeds when the frequency of the ice actions adapts to the frequency of the structural displacements at the waterline. The structural response in the lock-in range is in steady-state and is almost sinusoidal.
- **Continuous brittle crushing**. This scenario can occur at high interaction speeds. Here, the ice action and the structural response are random.

Frequency lock-in vibrations, often denoted as ice-induced vibrations (IIV), may cause fatigue damage to offshore structures, and they can disturb the working operation on those structures. Vertical structures are more vulnerable to IIV than sloping structures. There are different approaches to analyse and predict IIV. Some of the available methods are based on the idea of negative viscous damping, which is analogous to galloping. In addition, similarities between IIV and VIV can also be utilised, and models are currently being developed based on the idea of frequency and amplitude dependent added mass and added damping.

### 2.4.3 Level Ice Action on Sloping Structures

The interaction between level ice and sloping surfaces includes different processes and can be divided into several phases: breaking, rotating, sliding and clearing (or accumulating). Figure 2.5 illustrates in two dimensions the different phases of interaction between level ice and a bow of a ship-shaped floater, i.e., a sloping surface. The ice breaking phase begins with a localised crushing of the free ice edge at the contact zone. The crushing force increases as the structure penetrates into the ice and the contact area increases, which causes the ice sheet to deflect and the bending stresses to build up until the ice sheet fails.

A typical failure pattern will start with the formation of radial cracks in the ice sheet that are followed by a circumferential crack. If the contact area is quite wide, circumferential cracks may occur before the radial cracks; see Li et al. [15]. The flexural failure (circumferential crack) occurs at a distance from the crushing region. This distance, the breaking length, depends on the ice thickness and the ship speed, among other factors.

The broken ice pieces are often called cusps or wedges, depending on their geometry. Upon the formation of these cusps and wedges, the pieces start rotating downward until they are parallel to the sloping surface. During this rotation, the cusps and wedges push the previously broken ice pieces further down. Two important phenomena may occur in the rotating phase, depending on the speed of interaction. 1) Ventilation can arise if seawater is unable to immediately fill the gap above the rotating ice floes, which causes a substantial increase in the hydrostatic forces acting on the floes interacting with the structure, resulting in an increase in the global ice action. 2) The other phenomenon is that the structure may experience significant impact forces (slamming) at the end of the rotation phase due to the collision with the upper surface of the rotating ice floe. In the final phases of interaction, the broken ice pieces slide along the structure, and they may be cleared away or possibly accumulate around the structure. The interaction between sloping structures and ice floes in a broken ice field is slightly different from above, i.e., large ice floes may behave similar to level ice while smaller floes will mostly be pushed aside, rotated or submerged.

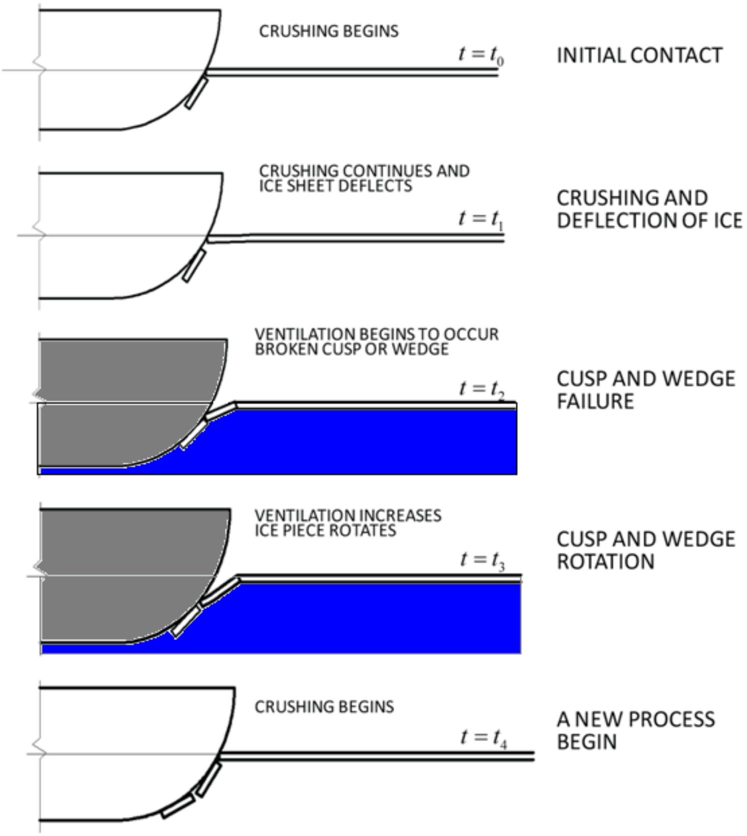
CRUSHING BEGINS
$t = t_0$
INITIAL CONTACT
CRUSHING CONTINUES AND ICE SHEET DEFLECTS
$t = t_1$
CRUSHING AND DEFLECTION OF ICE
VENTILATION BEGINS TO OCCUR BROKEN CUSP OR WEDGE
$t = t_2$
CUSP AND WEDGE FAILURE
VENTILATION INCREASES ICE PIECE ROTATES
$t = t_3$
CUSP AND WEDGE ROTATION
CRUSHING BEGINS
$t = t_4$
A NEW PROCESS BEGIN

Figure 2.5: Level-ice interaction with a sloping surface (figure reproduced from Kotras et al. [16]).

Valanto [17] studied the level ice resistance for ships moving in ice. He concluded that half of the resistance is the result of submerging the ice and the friction between the hull and the broken ice blocks travelling under the vessel. The other half of the resistance is caused by the processes at the waterline, including breaking the ice, accelerating the broken ice floes, ventilation, impact and stem crushing (see Figure 2.6). Croasdale et al. [18] presented a model to calculate the level ice action on wide conical structures, and this model was recently adopted by the ISO Code [2]. Croasdale divided the total ice force into five components (the breaking load is only one of them). Croasdale's model predicts the contribution of the breaking load component to be in the range of 20% to 30% of the total ice force.

Figure 2.6 shows that the global ice action (resistance) increases with the interaction speed. In fact, many field and model observations show similar speed effects; see Matskevitch [19]. The effects of the added mass and hydrodynamic damping from the water foundation under the ice are more significant at high interaction speeds than at low speeds. The rubble accumulation and clearance will also be influenced by the speed of interaction. Finally, high interaction speeds may change the mode of failure from bending to shear failure.

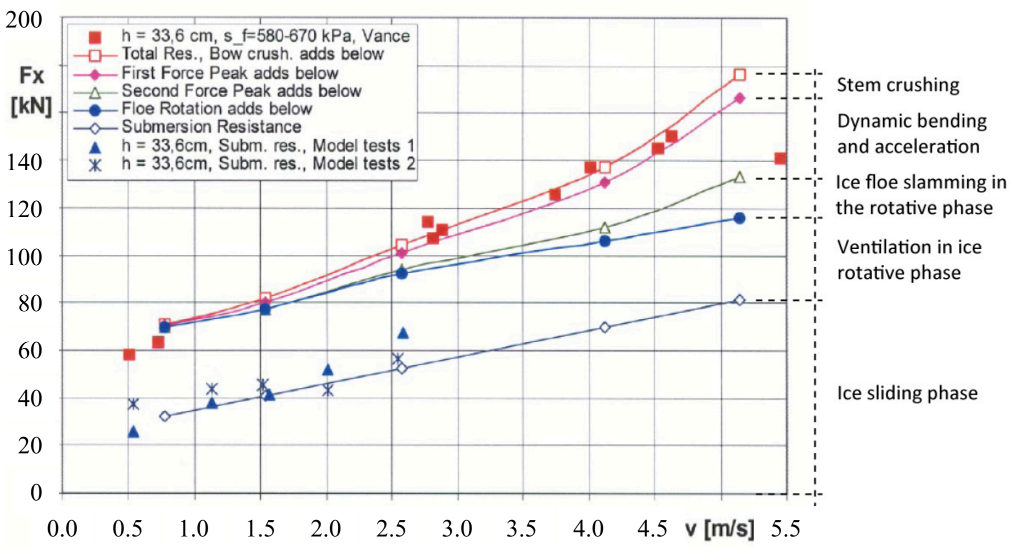

Figure 2.6: The contributions to the global ice actions (figure reproduced from Valanto [17]).

The response of structures, especially floaters, can have strong influence on the ice actions. A floater has six degrees of freedom (6 DOF), which translates mathematically into six coupled equations of motions written as

$$\sum_{k=1}^{6}\left[(M_{jk}+A_{jk})\ddot{\eta}_k + B_{jk}\dot{\eta}_k + C_{jk}\eta_k\right] = F_j \qquad (j = 1, \dots, 6) \qquad (2.12)$$

where $\eta_k$ are the floater motions: surge, sway, heave, roll, pitch and yaw. The dots denote time derivatives, i.e., $\dot{\eta}_k$ are the floater velocities, and $\ddot{\eta}_k$ are the floater accelerations. $M_{jk}$ and $A_{jk}$ are the components of the generalised mass and added mass matrices, respectively. $B_{jk}$ and $C_{jk}$ are the components of the damping and stiffness matrices, respectively. $F_j$ are the excitation forces and moments, which include, e.g., the ice actions.

Ice actions arise from interactions between the floater and ice. The contact forces between an ice floe and the floater are not known a priori but result from the balance between the floater motion and ice loading. The balance is often calculated by iterating the crushing depth. Another alternative is to couple the ice actions and the floater motion through a feedback loop, i.e., the current position of the ice and the previous position of the floater determine the contact forces at the present time step, and the calculated forces are used to modify the floater's position for the next time step.

The pitch motion of a floater, for example, may change the inclination angle of the structure against the ice, which will certainly affect the ice actions. If the pitch angle becomes sufficiently steep, the failure mode of ice may change from bending to shear or crushing, and this will significantly increase the ice actions on the floater and further increase its pitch angle. When the ice adjacent to the floater loses its integrity, the floater will try to return to its initial position, which may be accompanied by large accelerations that could hinder the operations or cause discomfort for the personnel working on the floater.

Ice vaning is a very important operation associated with the station keeping of floaters in the Arctic offshore. The floater must be heading against the ice drift direction to ensure that the ice will interact with the bow of the floater. Here, the accurate prediction of the floater response is essential for the reliability of such operations. Certain yaw angles can be sufficient for the ice to interact with the almost vertical sides of the floater. In this scenario, the ice forces on the floater side are very large, and it is quite challenging for the station-keeping system (both mooring and DP systems) to function properly.

## References:

[1] National Oceanic and Atmospheric Administration, U.S. Department of Commerce, http://oceanexplorer.noaa.gov/explorations/06mexico/background/oil/media/types_600.html, Revised August 26, 2010 by the Ocean Explorer Webmaster.

[2] ISO/CD 19906, 2010. Petroleum and Natural Gas Industries — Arctic Offshore Structures, ISOTC 67/SC 7/WG8. Final Draft International Standard. International Standardisation Organization, Geneva, Switzerland. 434 p.

[3] DNV-OSS-102, 2010. Rules for Classification of Floating Production, Storage and loading Units, Det Norske Veritas, 148 p.

[4] Gudmestad, O.T., Løset, S., Alhimenko, A. I., Shkhinek, K. N., Tørum, A., and Jensen, A., 2007. Engineering Aspects Related to Arctic Offshore Developments. “LAN”, ISBN 978-5-8114-0723-1, 256 p.

[5] Lever, G.V., Kean, J.R., and Muggerridge, K.J., 2001. Terra Nova FPSO on the Grand Banks of Canada. The 16th International Conference on Port and Ocean Engineering Under Arctic Conditions (POAC), Ottawa, Canada, pp. 3-20.

[6] Frankenstein, S., Løset, S., and Shen, H. H., 2001. Wave-Ice Interactions in the Barents Sea Marginal Ice Zone. ASCE Journal of Cold Regions Engineering, Vol. 15, No. 2, pp. 91-102.

[7] Zdravkovich, M.M., 1997. Flow Around Circular Cylinders, Vol. 1: Fundamentals. Oxford University Press, Oxford, England, 672 p.

[8] Zdravkovich, M.M., 2003. Flow Around Circular Cylinders, Vol. 2: Applications. Oxford University Press, Oxford, England, 1264 p.

[9] Blevins, R.D., 1994. Flow-Induced Vibration (Second ed.), New York, USA, Van Nostrand Reinhold, 477 p.

[10] Chakrabarti, S.K., 2002. The Theory and Practice of Hydrodynamics and Vibration, Advanced series on ocean engineering vol. 20, World Scientific Publishing Co. Pte. Ltd., River Edge, N.J., 464 p.

[11] Larsen, C.M., 2000. Empirical VIV Models, Workshop on Vortex-Induced Vibrations of Offshore Structures, Sao Paulo, Brazil.

[12] Zdravkovich, M.M., 1981. Review and classification of various aerodynamic and hydrodynamic means for suppressing vortex shedding, Journal of Wind Engineering and Industrial Aerodynamics, vol. 7, pp. 145-189.

[13] Jones, G.S., and Lamb, W.S., 1993. The suppression of vortex induced vibration in marine risers. Trans IMarE, vol. 105, Part 5, pp 197-209.

[14] Løset, S., Shkhinek, K.N., Gudmestad, O.T., and Høyland, K.V., 2006. Actions from Ice on Arctic Offshore and Coastal Structures. "LAN", ISBN S-8114-0703-3, 272 p.

[15] Li, F., Yue, Q.J., Shkhinek, K.N., and Kärnä, T., 2003. A Qualitative Analysis of Breaking Length of Sheet Ice Against Conical Structures. Proceedings of the 17th International Conference on Port and Ocean Engineering under Arctic Conditions, POAC '03, Trondheim, Norway,

[16] Kotras, T.V., Baird, A.V. and Naegle, J.N., 1983. Predicting Ship Performance in Level Ice. SNAME Transactions, Vol. 91, pp. 329-349.

[17] Valanto, P., 2001. The Resistance of Ships in Level Ice. SNAME Transactions, Vol. 109, pp. 53-83.

[18] Croasdale, K.R., Cammaert, A.B. and Metge, M., 1994. A Method for the Calculation of Sheet Ice Loads on Sloping Structures. IAHR 94, Proceedings of the 12th International Symposium on Ice, The Norwegian Institute of Technology, Trondheim, Norway, August 23-26, Vol. 2, pp. 874 – 885.

[19] Matskevitch, D.G., 2002. Velocity Effects on Conical Structure Ice Loads. Proceedings of 21st International Conference on Offshore Mechanics and Arctic Engineering (OMAE), Oslo, Norway, OMAE2002-28079.

# CHAPTER 3

## Closed-Form Solutions for Vibrations of Nearly Vertical Strings and Beams by Means of Asymptotic Methods

Is not included due to copyright

# CHAPTER 4

# Frequency and Mode Shape Estimates of Marine Catenary Systems using Asymptotic Approximations

# Frequency and Mode Shape Estimates of Marine Catenary Systems using Asymptotic Approximations

**Raed K. Lubbad**[1], **Geir Moe**[2] **and John M. Niedzwecki**[3]

## Abstract

Catenary configurations are commonly found in a wide range of offshore science and engineering applications, with the most common being the use of spread mooring systems for the station keeping of various floating platforms. Increasingly, attention has been focused upon predicting the susceptibility of catenary cables and marine risers to flow-induced vibrations. In this research study it is assumed that the dynamics of the catenary in the cross-flow direction can be determined without considering the motions in the in-line direction. A WKB analysis and another asymptotic method denoted ‘local analysis’ are then used as the basis to develop closed-form approximate solutions of the cross-flow natural frequencies and mode shapes for a catenary. The accuracy of these approximations is established through comparison with other analytic solution techniques and with results from numerical finite element solutions. The effects of bending stiffness and the effects of approximating the tension variation along the catenary by a linear function are discussed. Experimental data on the multi-modal in-line and cross-flow response behavior of a towed catenary model provides a means to illustrate the usefulness of the presented analytical asymptotic approximations in predicting the response frequencies and mode shapes due to the vortex induced vibrations.

***Keywords:*** catenary systems, mooring lines, steel catenary risers, asymptotic approximations, in-line response, cross-flow response, frequencies and mode shapes, model tests.

## 1. Introduction

Mooring lines and spread mooring systems are commonly used to provide station keeping for buoys, barges, ships and floating offshore platforms. More recently steel catenary risers (SCR) have become integral to the offshore petroleum industry and are typically used as flexible pipelines to transport oil and gas from the seafloor or as export flow-lines to transport fluids to storage or production facilities. Regardless of the application these long slender structural elements are often subject to harsh offshore environments. Therefore, a safe design of these structures requires a careful analysis to their dynamic response. Marine risers and mooring lines are often modeled as tension dominated cables or beams due to their line topology and the applied pretension. The dynamics of these models is complicated by non-linearities that may be due the geometry, the material properties, hydrodynamic forces, effects of structural interaction with the sea bed, or some combination of these factors. Mathematically, it is possible to formulate a set of nonlinear coupled partial differential equations to serve as the basis for dynamic analyses of catenary structures. For example, the three dimensional dynamic equations of cables were derived by Bliek [1], while the three

---

[1] Ph.D. candidate, Department of Civil and Transportation Engineering, NTNU, Trondheim Norway.
[2] Professor, Department of Civil and Transportation Engineering, NTNU, Trondheim Norway.
[3] Professor, Zachry Department of Civil Engineering, TAMU, College Station, TX, USA.

dimensional equations of beams with large deformation can be found in, for example, the doctoral thesis by Kim [2]. Depending upon the complexity of the model, numerical solutions may require a substantial computational time and depending on the numerical model they may only provide global quantitative response results and consequently little understanding as to the relative influences of the various parameters that govern the problem solution.

An alternate formulation that utilizes asymptotic methods can be used to derive analytical approximations for the eigen-frequencies and corresponding mode shapes of a catenary. As a consequence of initially assuming that the dynamic response is relatively small, the un-damped cable or beam formulations lead to distinct natural frequencies and mode shapes that depend only on the static configuration and the boundary conditions. The closed-form solutions for the eigenvalue problem can be useful in several ways: 1) it enhances the understanding of how the different structural parameters affect the structural response to the external loadings, 2) it simplifies the modal analysis of the structural response, 3) based upon these approximate solutions one can assess whether excitation from the environment is sufficiently near any natural frequencies of the catenary that the response could be amplified in the damping controlled region, potentially leading to undesirable acceleration of fatigue or other design problems, or in other words 4) it can be used for practical problems in order to assess whether higher order approximations or more complex analyses are needed to more adequately address relevant system nonlinearities.

Technical articles that are available in the open literature provide an ample source of information on the natural frequencies and mode shapes of cables with different geometries and boundary conditions, see for example Irvine and Caughey [3], Triantafyllou and Bliek [4] and Triantafyllou et al. [5]. In each of these mentioned technical publications the researchers utilized a linear two-dimensional theoretical approach to investigate the free vibrations of extensible cables. Based upon their analyses they concluded that the out-of-plane dynamic response was uncoupled from the in-plane response. However, the in-plane transverse and longitudinal motions were coupled and depended upon the ratio of elastic stiffness to catenary stiffness. Although the cable elastic waves were neglected in the article by Irvine and Caughey [3], the inclusion of elasticity in the equations of motion was enough to explain the frequency cross-over phenomenon and the symmetric/anti-symmetric modes in the in-plane dynamics of horizontal cables. By retaining the elastic waves it was possible to show the existence of hybrid modes in the in-plane motions of inclined cables (Triantafyllou and Bliek [4] and Triantafyllou et al. [5]). In addition, it was claimed that the catenary stiffness is dominant for inclined cables with large sag and consequently a pure catenary cable can well be modeled as an inextensible cable. Moe and Chucheepsakul [6] and Strømsem [7] studied the effects of internal flow on the eigenvalue problem solution and found out that under normal operating conditions the internal flow has no effects on the natural frequencies and mode shapes of nearly vertical cables and that for curved cables the internal flow has minor effects on the in-plane natural frequencies, while hybrid mode shapes can occur for high internal flow velocities. In this research study, the effects of internal flow are not addressed. When bending stiffness of the catenary risers and mooring lines is no longer negligible, the eigenvalue problem becomes more complicated. To the authors' knowledge, there exists no closed form solution for this general problem, and closed form solutions are available mainly for the case of nearly vertical beams, see Kim [2] and Lubbad and Moe [8].

A major concern in the development of offshore slender structures is the Vortex Induced Vibrations (VIV). These vibrations increase the drag forces and they may cause fatigue damage. Therefore, it is of utmost importance to accurately predict such vibrations and to have dependable methods by which to suppress them when necessary. Chaplin et al. [9]

compared laboratory measurements of VIV of a vertical tensioned riser with blind predictions of 11 different numerical models. It was shown there that the frequency domain models predicted the frequencies and mode shapes of vibrations well while the motion amplitudes were less well predicted. This is a good indicator that the closed-form solutions for the natural frequencies and mode shapes of vertical risers can indeed be useful in the analysis of VIV. The results from the vertical riser experiments encouraged the authors of this paper to study the similarities between the vertical and catenary configurations. In this study we first formulate the free-vibrations problem of a catenary in the cross-flow direction. Then we derive asymptotic solutions using local asymptotic analysis and WKB (Wentzel-Kramers-Brillouln) asymptotic methods. A numerical finite-element solution is described and used to verify the results of the asymptotic methods. Finally, the calculated frequencies and mode shapes are compared with laboratory measurements from an SCR model test program to verify the usefulness of the asymptotic solutions in predicting the VIV of catenary configurations.

## 2. Catenary Cross-flow Free Vibrations

The pure catenary shape which is formed by a flexible structural element hanging under the influence of its own weight and in the absence of any ocean waves or currents is illustrated in Figure 1. Initially the catenary shape is envisioned to lie in the two dimensional $x$-$z$ plane that has its origin where the catenary touches the seafloor that is the touch-down point (TDP). The Lagrangian coordinate $s$ that follows the catenary shape also has its origin at the TDP of the catenary. The out-of-plane displacement at any point along $s$ is $W$ while the in-plane tangential and normal displacements are $U$ and $V$ respectively. The suspended catenary length is $L$, the slope angle of the catenary is $\theta$, the applied top tension is $T_t$ and for a pure catenary shape the horizontal component of the static tension is constant along the catenary, that is $H = T_t \cos(\theta_t)$ where $\theta_t$ is the angle measured or observed as the catenary breaks the free surface of the ocean. Assuming that the catenary is simply supported at both ends researchers have obtained analytical expressions for the quasi-static response of the catenary, see for example Triantafyllou et al. [5], and Moe and Arntsen [10].

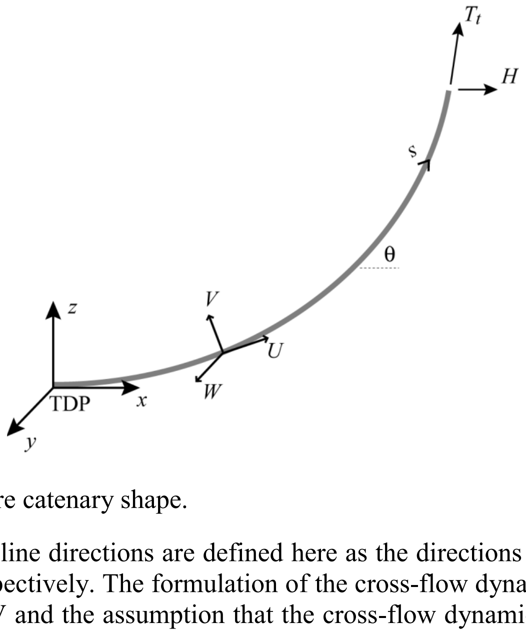

Figure 1: The basic pure catenary shape.

The cross-flow and in-line directions are defined here as the directions normal and parallel to the flow direction, respectively. The formulation of the cross-flow dynamics is very important for the analysis of VIV and the assumption that the cross-flow dynamics are uncoupled from the in-line dynamics is an important practical simplification of the problem. When the flow is in the plane of the catenary, the cross-flow direction becomes parallel to the catenary out-of-plane direction and the aforesaid assumption is widely accepted among researchers in the field of cable dynamics. When the flow acts at an oblique angle to the catenary plane, the assumption becomes questionable, especially for oblique angles close to 90º. When the effects of bending stiffness are dominating, the decoupling assumption will probably be about as accurate as the results for a long, slender, initially straight beam along the vertical axis (i.e. the $z$-axis) that experiences moderately large deflections. These equations as presented by Kim [2] are coupled through the nonlinear tension regardless of whether the bending stiffness is included. Analogously for the cable case, it seems reasonable to assume that even for the beam case the catenary cross-flow dynamics are decoupled from those in the in-line direction and this assumption is best when the flow is in the plane of the catenary. The equation for the cross-flow dynamics can then be approximated and expressed in terms of derivatives along the catenary as

$$\frac{\partial^2}{\partial s^2}\left(EI\frac{\partial^2 W}{\partial s^2}\right)-\frac{\partial}{\partial s}\left(T\frac{\partial W}{\partial s}\right)+m\frac{\partial^2 W}{\partial t^2}=f_y \tag{1}$$

where $s$ is as defined previously. $T$ is the static (effective) tension and it is a nonlinear function of $s$. $W$, as from here, is the displacement in the cross-flow direction (same as the catenary out-of-plane displacement when the flow is in the plane of the catenary). $t$ is the time, $EI$ is the bending stiffness, $f_y$ is the external loading in the cross-flow direction and $m$ is the total mass per unit length of the catenary, including external added mass effects (virtual mass).

## 3. First-Order Asymptotic Solution for a String Cross-flow Model

When the bending stiffness and the external loading are neglected, equation (1) reduces to the equation of a free vibrating string under a variable tension, i.e.

$$-\frac{\partial}{\partial s}\left(T\frac{\partial W}{\partial s}\right)+m\frac{\partial^2 W}{\partial t^2}=0 \tag{2}$$

For the case where the tension in the catenary structure is approximated by a linear function, exact solutions in terms of Bessel functions, as well as, asymptotic solutions are available, see for example Moe and Chucheepsakul [6]. Sparks [11] analyzed equation (2) under a linearly varying tension and estimated the of out-of-plane natural frequencies for steel catenary risers. On the other hand, one would expect better estimates of the natural frequencies and mode shapes if the nonlinear tension variation is considered. In the discussion that follows a so-called local analysis which is a form of an asymptotic solution method is used to derive closed form analytical solutions for the free vibration of a string model of a catenary structure with nonlinear tension variation.

The effective tension in a pure catenary slender structure varies nonlinearly as

$$T=H\sqrt{1+\alpha^2} \tag{3}$$

where, $\alpha=\alpha(s)=\tan\theta$. The time dependence in equation (2) is expected to be purely harmonic, suggesting a solution of the form

$$W(s,t)=w(s)\cos\omega t \tag{4}$$

and here $\omega$ is the natural frequency of the catenary structure. Equation (4) basically suggests a separation of variables where $W(s,t)$ is written as a function of space only, $w(s)$, multiplied by a function of time. For convenience of notation, $w(s)$ is simply written as $w$ in the following text. Substituting equation (4) into equation (2) and utilizing the relationship $\alpha = \tan\theta = \tau \cdot s/L$ where $\tau$ is the value of $\tan\theta$ at $s = L$ one obtains an equation of the form

$$\frac{\partial}{\partial\alpha}\left(T\frac{\partial w}{\partial\alpha}\right) + m\Lambda^2 w = 0 \qquad (5)$$

where, $\Lambda = \omega L/\tau$. From which it follows that

$$w'' + \frac{\alpha}{1+\alpha^2}w' + \frac{\zeta\Lambda^2}{\sqrt{1+\alpha^2}}w = 0 \qquad (6)$$

and the primes denote differentiation with respect to $\alpha$ and $\zeta = m/H$.

The asymptotic method known by the name “local analysis” can now be used to solve equation (6). First the solution is assumed on the form $w = e^{S(\alpha)}$ where upon substitution into equation (6) yields

$$S'' + S'^2 + \left(\frac{\alpha}{1+\alpha^2}\right)S' + \frac{\zeta\Lambda^2}{\sqrt{1+\alpha^2}} = 0 \qquad (7)$$

Assuming that $S'' \ll S'^2$, see Bender & Orszag [12], one can solve the resulting quadratic equation in $S'$ and for large values of $\alpha$, i.e. $\alpha \to \infty$, one obtains the solution

$$S' \sim -\frac{1}{2}\left(\frac{\alpha}{1+\alpha^2}\right) \pm i\Lambda\sqrt{\zeta}(1+\alpha^2)^{-\frac{1}{4}}, \qquad \alpha \to \infty \qquad (8)$$

Integrating equation (8) with respect to $\alpha$, the solution takes the form

$$S = S_0 + C(\alpha) \qquad (9)$$

where, $C(\alpha)$ is an integration function of lower order in $\alpha$ (much smaller in the limit than $S_0$) and one finds that

$$S_0 = -\frac{1}{4}\ln(1+\alpha^2) \pm i\Lambda\sqrt{\zeta}\int^{\alpha}(1+\alpha^2)^{-\frac{1}{4}}\,d\alpha \qquad (10)$$

By neglecting $C(\alpha)$ a first-order approximation to the solution of equation (6) can be written as

$$\begin{aligned} w \sim\ & \tilde{A}\cdot(1+\alpha^2)^{-\frac{1}{4}}\cdot e^{i\Lambda\sqrt{\zeta}\left(\int^{\alpha}(1+\alpha^2)^{-\frac{1}{4}}d\alpha\right)} \\ & + \tilde{B}\cdot(1+\alpha^2)^{-\frac{1}{4}}\cdot e^{-i\Lambda\sqrt{\zeta}\left(\int^{\alpha}(1+\alpha^2)^{-\frac{1}{4}}d\alpha\right)} \end{aligned} \qquad (11)$$

where, $\tilde{A}$ and $\tilde{B}$ are constants. Noting that the integral is always real since $\alpha$ is real, the exponential functions in equation (11) can more conveniently be expressed in terms of trigonometric functions, and it follows that

$$
\begin{aligned}
w \sim A \cdot (1+\alpha^2)^{-\frac{1}{4}} \cdot \sin\left(\Lambda\sqrt{\zeta}\int^{\alpha}(1+\alpha^2)^{-\frac{1}{4}}d\alpha\right) \\
+ B \cdot (1+\alpha^2)^{-\frac{1}{4}} \cdot \cos\left(\Lambda\sqrt{\zeta}\int^{\alpha}(1+\alpha^2)^{-\frac{1}{4}}d\alpha\right)
\end{aligned}
\tag{12}
$$

where, again $A$ and $B$ are constants. The boundary conditions for the simply supported case are:

$$
\begin{aligned}
&w(s=0) = w(\alpha=0) = 0 \\
&w(s=L) = w(\alpha=\tau) = 0
\end{aligned}
\tag{13}
$$

Equation (12) will satisfy the above boundary conditions only if

$$
\begin{aligned}
&B = 0 \\
&\Lambda_n\sqrt{\zeta}\int_0^{\tau}(1+\alpha^2)^{-\frac{1}{4}}d\alpha = n\pi, \qquad n = 1,2,3\,...
\end{aligned}
\tag{14}
$$

Thus, *the first-order asymptotic solution for the mode shapes* becomes

$$
w_n \sim (1+\alpha^2)^{-\frac{1}{4}} \cdot \sin\left(\frac{\omega_n L}{\tau}\sqrt{\zeta}\int_0^{\alpha}(1+\alpha^2)^{-\frac{1}{4}}d\alpha\right) \tag{15}
$$

and *the corresponding first-order natural frequencies* $\omega_n$ can be calculated from the second in equation (14) as:

$$
\omega_n = \frac{\tau}{L} \cdot \frac{n\pi}{\sqrt{\zeta}}\left(\int_0^{\tau}(1+\alpha^2)^{-\frac{1}{4}}\,d\alpha\right)^{-1} \tag{16}
$$

The integration of the integrals in equations (15) and (16) is more suitable for numerical evaluation. Alternatively one can derive an approximate closed form solution by expanding the function $(1+\alpha^2)^{-\frac{1}{4}}$ around $\alpha = \infty$. It follows then that, the integral $\int_0^{\tau}(1+\alpha^2)^{-\frac{1}{4}}d\alpha$ can be approximated to a maximum error of less than 0.2%, by the following expression

$$
\frac{1}{\sqrt{2}}\left[2e^{\epsilon/2} - \frac{1}{3}e^{-3\epsilon/2} + \frac{1}{28}e^{-7\epsilon/2} - \frac{1}{88}e^{-11\epsilon/2} + \frac{1}{192}e^{-15\epsilon/2} - \frac{8359}{4928}\right] \tag{17}
$$

where $\epsilon = \sinh^{-1}(\tau)$.

## 4. Second-Order Asymptotic Solution for a String Cross-flow Model

Further improvement to the first-order asymptotic solution for the natural frequency and mode shape estimates can be achieved by evaluating the term $C(\alpha)$ in equation (9). Substitute equation (9) into equation (7) one obtains the following equation

$$
S_0'' + C'' + S_0'^2 + 2S_0'C' + C'^2 + \left(\frac{\alpha}{1+\alpha^2}\right)\left(S_0' + C'\right) + \frac{\zeta\Lambda^2}{\sqrt{1+\alpha^2}} = 0 \tag{18}
$$

Next the terms $C''$ and $C'^2$ can be neglected since $C$ is much smaller than $S_0$. The other terms, $S_0'^2$ and $S_0''$, are calculated using equation (10) as

$$S_0^{''} = \left[-\frac{1}{2(1+\alpha^2)} + \frac{\alpha^2}{(1+\alpha^2)^2}\right] \mp \frac{i\Lambda\sqrt{\zeta}\alpha}{2(1+\alpha^2)^{\frac{5}{4}}}$$

$$S_0^{'2} = \frac{\alpha^2}{4(1+\alpha^2)^2} - \frac{\zeta\Lambda^2}{(1+\alpha^2)^{\frac{1}{2}}} \mp \frac{i\Lambda\sqrt{\zeta}\alpha}{(1+\alpha^2)^{\frac{5}{4}}} \tag{19}$$

Equation (18) can now be solved for the only remaining unknown, $C'$, yielding

$$C' = \frac{\alpha}{4(1+\alpha^2)} \pm i\frac{(\alpha^2-2)}{8\Lambda\sqrt{\zeta}(1+\alpha^2)^{\frac{7}{4}}} \tag{20}$$

Integrating equation (20) one obtains the second-order correction term

$$C(\alpha) = \frac{1}{8}\ln(1+\alpha^2) \pm i\frac{1}{8\Lambda\sqrt{\zeta}}\int_0^{\alpha}\frac{(\alpha^2-2)}{(1+\alpha^2)^{\frac{7}{4}}}d\alpha \tag{21}$$

Thus, the earlier expression, equation (9) can now be replaced by the expression

$$S = S_0 + C(\alpha) + g(\alpha) \tag{22}$$

where, $g(\alpha)$ is again an integration function much smaller than the second-order correction term. Neglecting $g(\alpha)$ and solving for the mode shape and frequency expressions, one obtains the following *second order approximation for the mode shapes*

$$w_n \sim \chi^{-\frac{1}{4}} \cdot \sin\left(\frac{\omega_n L}{\tau}\sqrt{\zeta}\int_0^{\alpha}\chi^{-\frac{1}{2}}d\alpha + \frac{\tau}{8\omega_n L\sqrt{\zeta}}\int_0^{\alpha}\frac{(\chi^2-3)}{(\chi)^{\frac{7}{2}}}d\alpha\right) \tag{23}$$

where

$$\chi = \sqrt{1+\alpha^2} \tag{24}$$

The corresponding natural frequencies are the values of $\omega_n$ which make the argument of the sine function in equation (23) equal to $n\pi$. Unfortunately, it is not possible to solve this explicitly and the *second order approximation for the natural frequencies* can only be estimated by solving the following equation for $\omega_n$ iteratively.

$$\frac{\omega_n L}{\tau}\sqrt{\zeta}\int_0^{\tau}\chi^{-\frac{1}{2}}d\alpha + \frac{\tau}{8\omega_n L\sqrt{\zeta}}\int_0^{\tau}\frac{(\chi^2-3)}{(\chi)^{\frac{7}{2}}}d\alpha = n\pi \tag{25}$$

Triantafyllou and Bliek [4] solved the cable out-of-plane dynamics using the WKB method and interestingly their final results for the natural frequencies are the same as the first order approximations presented in this discussion. Pesce et al. [13] used the WKB method in order to study the *in-plane dynamics* of catenary cables. However, after neglecting most of the nonlinear terms, their problem of the transverse in-plane motion became identical to the problem discussed here for the cross-flow dynamics. As were to be expected, Pesce et al. [13] arrived at the exact same result as our first-order approximation. Later in this paper, numerical examples will compare the effects of linear and nonlinear tension variations on the natural frequencies and mode shapes of a catenary. The examples will also be used to compare the accuracy of the first and second order approximations derived here.

## 5. Asymptotic Solutions for a Beam Cross-flow Model

This section discusses the solutions to the problem of free vibrating beam under varying tension, i.e., solutions to equation (1) when $f_y = 0$. This discussion is useful for studying the effects of bending stiffness on the cross-flow dynamics of catenary slender structures. Here the structures of interest are uniform, i.e. the bending stiffness and the mass per unit length are constant. Assuming that the tension is continuous and varies nonlinearly but slowly along the structure, Kim [2] used the WKB method and provided an asymptotic solution to equation (1). Later Lubbad and Moe [8] studied the free vibrations of beams under linearly varying tension. In their study they showed how the WKB solution could be improved and by performing the integrations analytically, thus simplifying the final results and allowing the higher order approximations to the slope and bending moment. They also improved upon the numerical stability of the WKB solution by replacing the hyperbolic sine and cosine with exponential functions that originated at the boundaries and decreased uniformly away from these. For a simply supported beam *the mode shapes* as presented by Lubbad and Moe [8] are

$$w_n = \frac{e^{(\xi_n/4)}}{\sqrt{\cosh(\xi_n)}} \sin\left(\frac{\Gamma_n^{\ 1.5}}{b}\left(2e^{(\xi_n/2)} - \frac{2}{3}e^{(-3\xi_n/2)}\right)\Bigg|_{\xi_{n_b}}^{\xi_n}\right) \tag{26}$$

and *the corresponding natural frequencies* are the roots of the following equation.

$$\frac{\Gamma_n^{\ 1.5}}{b}\left(2\mathrm{e}^{(\xi_n/2)} - \frac{2}{3}\mathrm{e}^{(-3\xi_n/2)}\right)\Bigg|_{\xi_{n_b}}^{\xi_{n_t}} = n\pi \tag{27}$$

The variables in the above two equations are defined as follows

$$\begin{gathered} a = \frac{HL^2}{EI}, \qquad b = \frac{(T_t - H)L^2}{EI}, \qquad \Gamma_n = \frac{\omega_n}{\omega_0}, \qquad \omega_0 = \sqrt{\frac{EI}{mL^4}}, \qquad \check{s} = \frac{s}{L} \\ \xi_n = \sinh^{-1}\left(\frac{a + b\check{s}}{2\Gamma_n}\right), \qquad \xi_{n_b} = \xi_n(\check{s} = 0), \qquad \xi_{n_t} = \xi_n(\check{s} = 1), \end{gathered} \tag{28}$$

where as before $s$ is the lagrangian coordinate along the catenary, $L$ is the suspended length of the catenary, $H$ is the effective tension at the TDP, $T_t$ is the effective tension at the top end, $EI$ is the bending stiffness, $\omega_n$ is the natural frequencies and $m$ is the virtual mass per unit length. The tension of catenary structures, equation (3), varies nonlinearly but fairly slowly. This satisfies the inherent assumption in the solution of Kim [2]. As shown later by the numerical examples, the effective tension can be approximated by a linear function and equations (26) and (27) yield quite good results.

## 6. Finite Element Solutions

The un-damped cross-flow natural frequencies and mode shapes of a catenary can be calculated by discretizing the catenary into a number of elements. The governing differential equation of each element is described as:

$$\frac{\partial^2}{\partial \bar{z}^2}\left(EI\frac{\partial^2 v}{\partial \bar{z}^2}\right) - \frac{\partial}{\partial \bar{z}}\left(T\frac{\partial v}{\partial \bar{z}}\right) + m\frac{\partial^2 v}{\partial t^2} = f_{\bar{y}} \tag{29}$$

where $\bar{z}$ and $\bar{y}$ are the element axial and transverse local coordinates respectively and $\bar{y}$ is parallel to the cross-flow direction. Cheng et al. [14] used the WKB solution for equation (29) and established the so called WKB-based dynamic element stiffness matrix as an alternative to the conventional finite element mass and stiffness matrices. This hybrid method presents a way of utilizing the asymptotic solutions in the finite element formulations but may be of limited practical significance otherwise. Therefore here is used a more traditional finite element method where each element has two nodes and three degrees of freedom at each node ($u$, $v$ and $\varphi$). The element dynamic equation can be written as

$$\begin{gathered}[m_e]\{\ddot{e}\} + [k_e]\{e\} = \{F\} \\ \{e\} = [u_1 \quad v_1 \quad \varphi_1 \quad u_2 \quad v_2 \quad \varphi_2]^T \\ \{F\} = [F_{\bar{z}1} \quad F_{y1} \quad M_1 \quad F_{z2} \quad F_{\bar{y}2} \quad M_2]^T\end{gathered} \tag{30}$$

where, the double dots denote the second derivative with respect to time and, $u$, $v$ and $\varphi$ are the axial, transverse and rotational degree of freedom, respectively. Since $\bar{y}$ is parallel to the cross-flow direction, $u$ would then represent the element stretching while $v$ and $\varphi$ would be the element displacement and rotation in the cross-flow direction, respectively. The equation variables $F_{\bar{z}}$, $F_{\bar{y}}$ and $M$ are the axial force, the shear force and bending moment, respectively and, the subscripts indicate the element node number. The local virtual mass matrix is $[m_e]$ and, the local stiffness matrix is $[k_e]$. The coupling on element level between the axial and transverse motions is neglected since the structure as a whole will accommodate axial deformation mainly by readjusting its static configuration and allowing a slight degree of stretching.

The stiffness matrix is the sum of the bending and the geometrical stiffness. When the tension is assumed constant within the element, the derivations of the mass and stiffness matrices is rather simple, see Kwon and Bang [15]. Somewhat improved results are obtained when the tension variation within the element is considered. Moe at al. [16] show how the stiffness matrix can be modified to account for a linear tension variation. Naturally, the next step is to assemble the global mass and stiffness matrices ($[M_G]$ and $[K_G]$, respectively) and the cross-flow free vibration equation becomes

$$([K_G] - \omega^2[M_G])\{E\} = 0 \tag{31}$$

and $\{E\}$ is the global assembly of the element displacements $\{e\}$. Equation (31) is an eigenvalue problem and can easily be solved for the natural frequencies and the corresponding mode shapes. Note that $[K_G]$ and $[M_G]$ must be modified to account for the proper boundary conditions. The finite element method explained above is quite general and can easily be adjusted to solve for the in-plane dynamics of a catenary and also for beam or cable cases.

The un-damped problem discussed above can in all but some very special cases be diagonalized so that ends up with a number of one-degree of-freedom equations. From each of these natural frequencies and mode shapes can easily be determined. When damping is added to the mass and stiffness terms in equation (30) diagonalization is strictly speaking not possible, but various approximate solutions are available. One may e.g. assume that the damping matrix is proportional to the stiffness or mass matrices or to a sum of two such terms. Often this is not a problem, since the full damping matrix cannot be determined anyway, while it may be possible to make a reasonable estimate of the modal damping for the most interesting modes. However there exists a method in which one can find the damped modes exactly. The essential difference for this case is that it permits the eigenvector to contain phase differences as well as the modal shape which now is an envelope, thus one can model travelling waves as well as standing waves. This vector is conveniently expressed by means of complex numbers and this technique is therefore often denoted as the use of complex modes. Phase differences will occur when the net energy balance is positive for one part of the system and negative in other parts. In some systems the term proportional to structural velocity $[C_e]\{\dot{e}\}$ may in addition to damping also represent so-called gyroscopic terms. Therefore the complex mode technique is in general quite useful and its main drawback is that it leads to the solution of an eigenvalue problem of a doubled number of degrees of freedom, which is with today's computational tools not a problem. The details of this technique may be found in Meirovitch [17] and some information about its application is found in Moe and Hoen [18].

## 7. Numerical Example

The above solutions of the cross-flow free vibrations of a catenary will be illustrated by means of an example. Table 1 presents the input data for the example. The data in Table 1 are taken from an SCR model test program, see Lie [19]. The details of these experiments and the analysis of the experimental data are discussed later in this paper.

Table 1: Riser main data (Lie [19]).

| | | |
|---|---|---|
| Total length between pinned ends | 12.5 m | |
| Mass per unit length including content | 0.357 kg/m | (1) |
| Outer diameter | 14 mm | |
| Wall thickness of riser | 0.45 mm | |
| Density of brass | 8980 kg/m$^3$ | (2) |
| Young modulus of brass | $1.5 \cdot 10^{11}$ N/m$^2$ | (2) |
| Axial stiffness | $2.01 \cdot 10^{6}$ N | (2) |
| Bending stiffness | 46.2 Nm$^2$ | (2) |
| Percent relative damping in air | 0.2 - 0.6 | |
| Horizontal distance between riser ends | 9.253 m | |
| Vertical distance between riser ends | 7.13 m | |
| Tension, upper end | 22.55 N | (3) |
| Tension, lower end | 8.44 N | (3) |
| Angle from vertical, upper end | 26° | (3) |
| Angle from vertical, lower end | 88° | (3) |

(1) This corresponds to an equivalent density of pipe content of 1373 kg/m$^3$ and density of the pipe with content of 2320 kg/m$^3$
(2) Nominal value
(3) Calculated by the program RIFLEX (Finite element model with beam elements)

### 7.1. String Model

The eigenvalue analysis requires the determination of the static configuration as the first step. The boundary conditions of the catenary are simply supported. Therefore, the complete static configuration can be calculated analytically by specifying only the total length, the vertical distance between the two ends and the cross-section properties of the catenary. Figure 2 shows the calculated static configuration of the pure catenary cable and it compares the nonlinear tension variation along the catenary to a linear approximation of the tension.

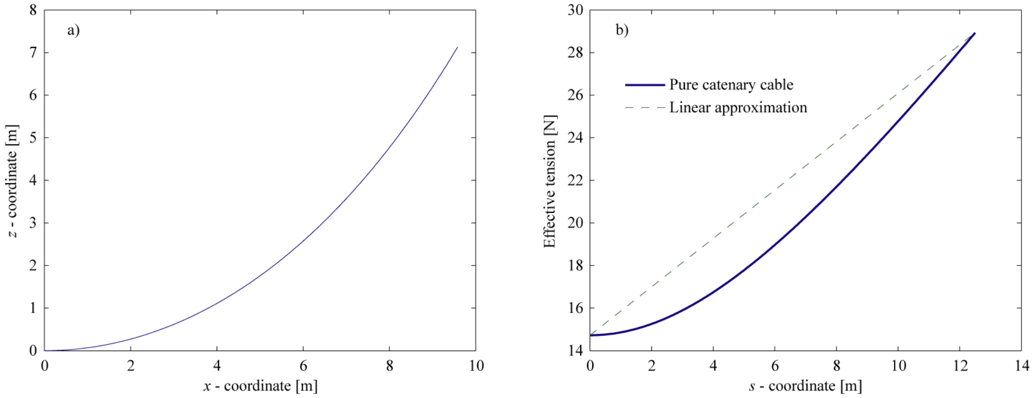

Figure 2: The results of the static analysis using the sting model, (a) Static configuration, (b) Comparison between the calculated nonlinear tension and a linear approximation.

In the analysis that follows the added mass coefficient is set equal to 1. Table 2 shows the cross-flow natural frequencies calculated using the string model. The calculations utilized the asymptotic expressions and an in-house Matlab program that uses the finite element solution described in this paper. The first cross-flow mode shape calculated by the different methods is shown in Figure 3.

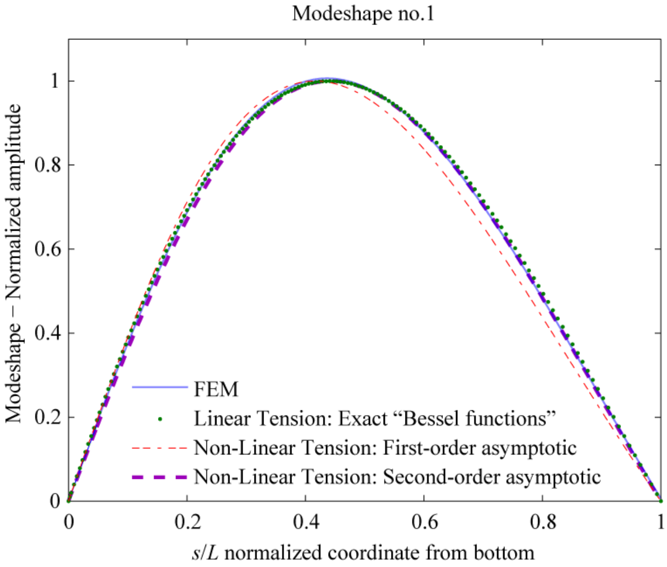

Figure 3: The cross-flow mode shape # 1 calculated using the sting model.

Table 2: Cross-flow natural frequencies [rad/s] calculated using the string model.

| Mode # | FEM | Percent difference in the analytical solutions: Linear Tension | | | Percent difference in the analytical solutions: NON-Linear Tension | |
|---|---|---|---|---|---|---|
| | In-house MATLAB program | Bessel functions Ref. [6] | Asymptotic [1 term] Ref. [6] | Asymptotic [2 terms] Ref. [6] | First-order (Eq. 16) | Second-order (Eq. 25) |
| 1 | 1.5688 | 3.13 | 3.28 | 3.12 | -1.22 | 0.99 |
| 2 | 3.1095 | 4.17 | 4.21 | 4.17 | -0.33 | 0.24 |
| 3 | 4.6558 | 4.38 | 4.40 | 4.38 | -0.15 | 0.11 |
| 4 | 6.2037 | 4.46 | 4.47 | 4.46 | -0.08 | 0.06 |
| 5 | 7.7524 | 4.49 | 4.50 | 4.49 | -0.05 | 0.04 |
| 6 | 9.3013 | 4.51 | 4.51 | 4.51 | -0.04 | 0.03 |
| 7 | 10.8505 | 4.52 | 4.52 | 4.52 | -0.03 | 0.02 |
| 8 | 12.3998 | 4.53 | 4.53 | 4.53 | -0.02 | 0.02 |
| 9 | 13.9492 | 4.53 | 4.53 | 4.53 | -0.02 | 0.01 |
| 10 | 15.4986 | 4.54 | 4.54 | 4.54 | -0.01 | 0.01 |

From the data in Table 2 and Figure 3 it seems that the linear approximation of the tension gives quite satisfactory results (the average percent difference is about 4%). On the other hand, using the nonlinear variation of the tension improved the results (percent difference varied from about 1% in the first mode to about 0.01% in the tenth mode). Again considering the nonlinear tension case, the second order asymptotic solution improved the mode shape but had little effects on the natural frequencies compared to the first order asymptotic solution.

### 7.2. Beam Model

The bending stiffness modifies the static configuration and that affects the calculation of the natural frequencies and mode shapes of the catenary. Figure 4 compares the static configuration of the beam model to that of the string model. The beam static configuration is calculated using the finite element software RIFLEX since the available analytical closed form solutions deal only with the string case.

As seen from Figure 4, the bending stiffness has noticeable effects on the static configuration which indicates that the results of the dynamic analysis for this example will be quite different if one uses the beam model instead of the string model. Another measure for the effects of bending stiffness on the dynamics of the risers can be obtained by calculating the nondimensional number, $\lambda_n$, suggested by Moe et al. [16]. The bending is important if $\lambda_n$ is order one or smaller.

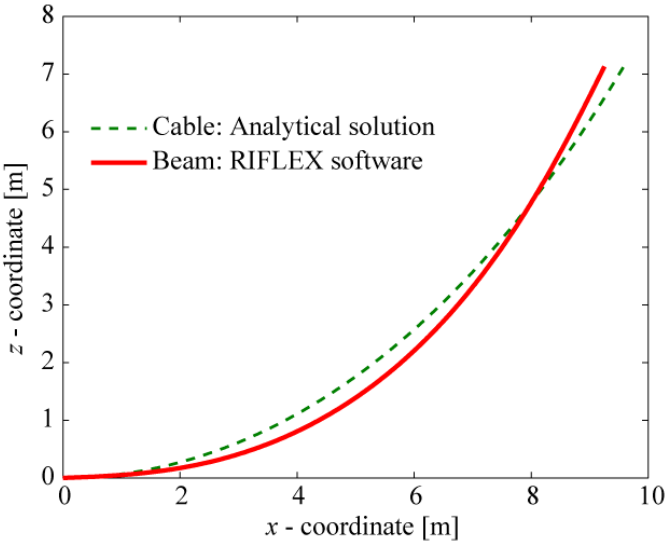

Figure 4: The static configuration of the catenary model: beam vs. string.

$$\lambda_n = \frac{\left(0.5 \cdot \left(\sqrt{H} + \sqrt{T_t}\right)\right)^2 \cdot L^2}{n^2 \cdot \pi^2 \cdot EI} \tag{32}$$

Using the input data from Table 1, $\lambda_n$ for $n \geq 3$ is always less than 1. This means that in the present problem, starting from the third mode, the bending stiffness is expected to have significant effects on the natural frequencies and mode shapes. Table 3 shows the cross-flow natural frequencies calculated using the beam model. The first cross-flow mode shape is shown in Figure 5.

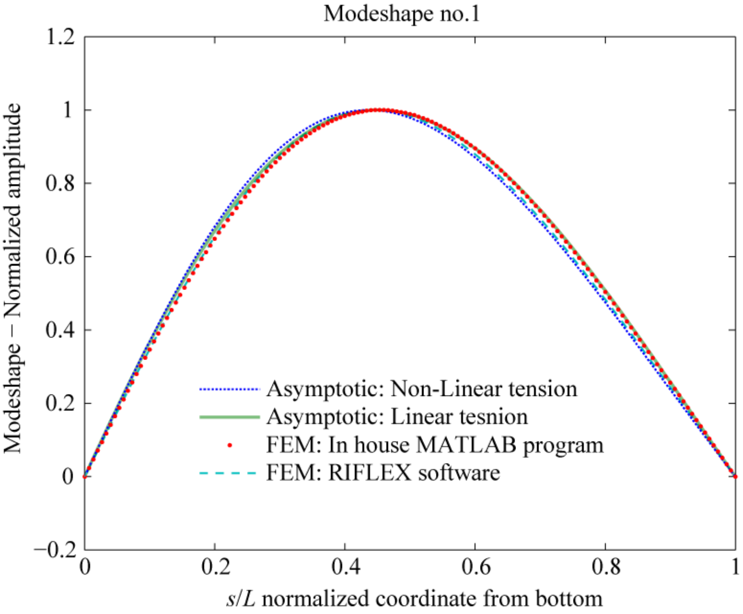

Figure 5: The cross-flow mode shape # 1 calculated using the beam model.

Table 3: Cross-flow natural frequencies [rad/s] calculated using the beam model.

| Mode # | FEM | | Analytical solutions | |
|---|---|---|---|---|
| | RIFLEX software | In house MATLAB program | Linear Tension (Eq.27) | Non Linear Tension Ref. [2] |
| **1** | 1.3692 | 1.4235 | 1.4908 | 1.4830 |
| **2** | 3.4136 | 3.5075 | 3.6556 | 3.6570 |
| **3** | 6.5069 | 6.6285 | 6.8132 | 6.8215 |
| **4** | 10.758 | 10.8881 | 11.0910 | 11.1030 |
| **5** | 16.186 | 16.3229 | 16.5359 | 16.5499 |
| **6** | 22.808 | 22.9468 | 23.1659 | 23.1811 |
| **7** | 30.626 | 30.7658 | 30.9887 | 31.0047 |
| **8** | 39.642 | 39.7825 | 40.0080 | 40.0245 |
| **9** | 49.857 | 49.9984 | 50.2257 | 50.2426 |
| **10** | 61.273 | 61.4142 | 61.6429 | 61.6600 |

The results in Table 3 and Figure 5 suggest that it is possible to approximate the tension in a catenary by a linear function and equations (26) and (27) would still yield quite good results for cross-flow natural frequencies and mode shapes.

## 8. Particulars of the Catenary Riser Experiments

An industry test program was conducted to investigate the coupled in-line and cross-flow induced response behavior on an instrumented catenary model subject to uniform flow. The intent was to gain insight into the dynamic behavior of steel catenary risers (SCRs) and to evaluate the ability of numerical models to correctly predict the observed behavior. The test model was affixed to a towing carriage and was designed to allow the angular orientation of the catenary model with respect to the towing carriage direction to be varied along with the towing speed.

As the model test program was designed to gain basic insight the model scale did not represent any particular offshore SCR, and the ratio of the length to diameter was approximately 890 which was noted to be less than what was typical of actual deepwater systems. Ten equally-spaced bi-axial accelerometers, as depicted by the circles along the static catenary curves in Figure 6 were affixed to the SCR model and they were sequentially numbered starting from the lower end of the catenary curve. In this study, the towing carriage speed will be used along with the bi-axial displacement information processed from the acceleration measurements. The three force components measured at both of the fixed ends is not addressed in this study. The model tests were conducted in a towing tank that was 80 m long, 10.5 m wide and 10 m deep, Lie [19]. The catenary model was 12.5 m long and had a diameter of 14 mm. The ratio of the horizontal to vertical projection was approximately 1.3. The model was towed at speeds ranging from 0.12-0.26 m/s at orientations of 0, 30, 60 and 90 degrees. Additional details of the experiment can also be found in the article by Moe et.al [20].

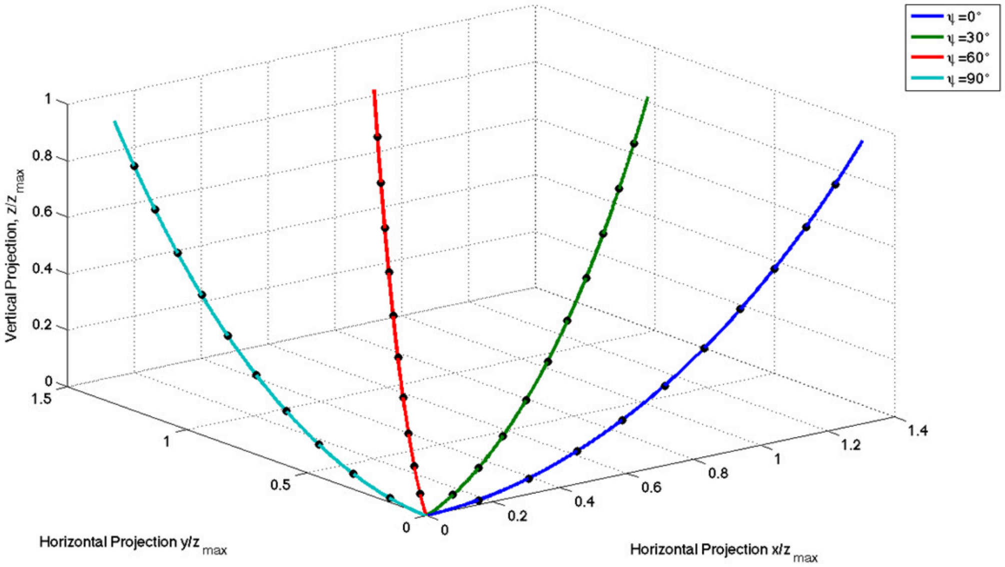

Figure 6: The experimental model test program. The riser is tested at the indicated 4 cases determined by $\psi$, i.e. the angle between the plane through the caternary and the flow direction.

## 9. Experimental Results and Discussions

The particulars of the experiments are described above and the main data of the catenary model are shown in Table 1. The measurements were taken at ten different locations along the catenary and the model was towed with four different speeds at four different orientations. This accumulated a huge amount of data, e.g., time series, spectral densities and motion envelops. Due to space limitation in this paper, only the few cases shown in Table 4 are selected for discussion. More details about the data analysis can be found in the articles by Niedzwecki and Moe [21] and Niedzwecki and Moe [22].

Table 4: The experimental cases selected for discussion.

| Towing speed [m/s] | Orientation | | | |
|---|---|---|---|---|
| | 0º | 30º | 60º | 90º |
| 0.12 | × | | | |
| 0.24 | × | | | |
| 0.26 | × | × | × | |
| 0.34 | × | | | |

Figure 7 shows a sample of the measured time series of the catenary displacements. These displacements were measured at the middle of the catenary, i.e., at accelerometer # 5. The towing speed was 0.26 m/s and the orientation angle was 0°, i.e. the flow was in the plane of the catenary. In the figure the displacements are divided by $D$, which is the diameter of the catenary.

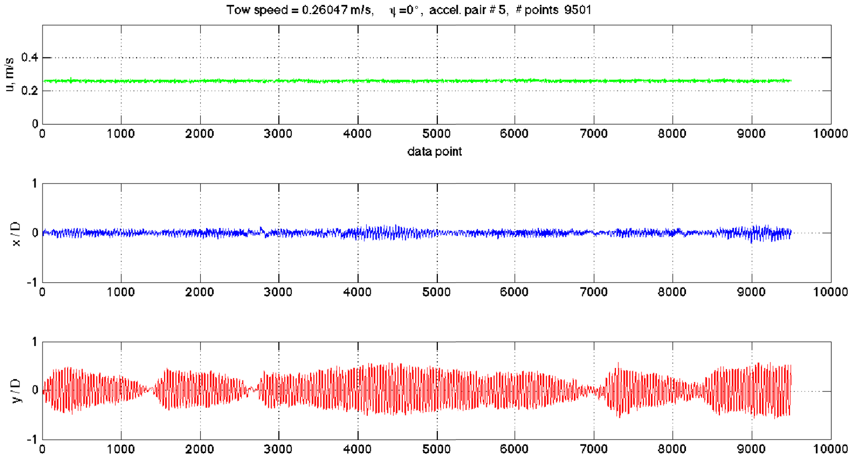

Figure 7: The motion in the $x$ and $y$ directions of accelerometer #5 on the catenary model.

It is seen from figure 7 that the displacements in the in-line direction (i.e. the $x$-direction) are very much smaller than for the transverse direction. If the time scale is increased sufficiently one would see that fairy regular sinusoidal motions occur. From figure 7 is also seen that the transverse motions at this location varies significantly with time, building up to amplitudes somewhat smaller than one half diameter over several motion periods, and then reducing very gradually back to almost zero motions for a few periods, i.e. the motion pattern at this point could be described as a modulated sine curve.

Figure 8 shows the spectral densities for the case of 0.26 m/s towing speed and 0° orientation angle. The left side of Figure 8 is calculated from measured vibrations near the lower end of the catenary while the right side of the figure is calculated from measured vibrations near the top of the catenary. Figure 8 shows that the vibrations in the cross-flow direction are dominated by a single frequency component. Minor contributions from other distinct frequencies were also present apparently occurring at integer multiples or fractions of the dominating component, indicating that the response of the catenary to VIV has super or sub-harmonic components. The spectral densities for the rest of the cases (see Table 4) are quite similar to those shown in Figure 8. Table 5 summarizes the measured dominant vibration frequencies in the cross-flow direction for the six selected cases.

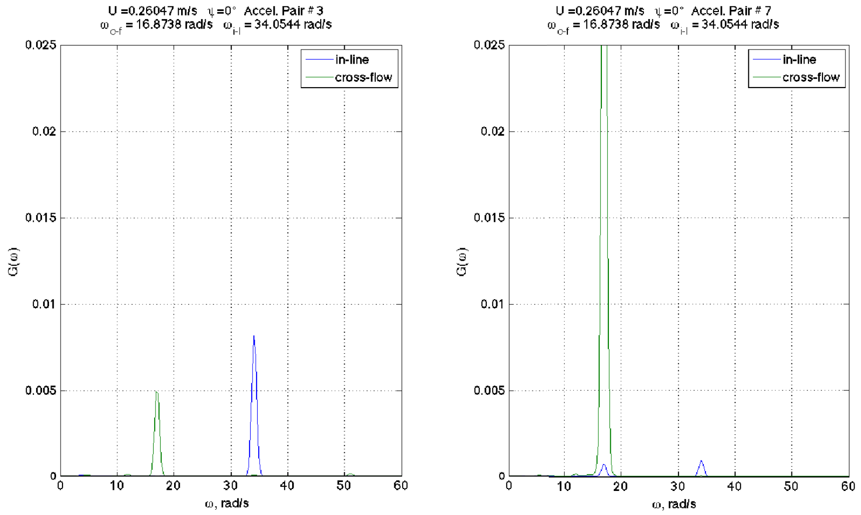

Figure 8: Spectral densities of the cross-flow and in-line vibrations of the experimental catenary model for the case of 0.26 m/s towing speed and 0° orientation angle.

Table 5: The measured dominant vibration frequencies in the cross-flow direction.

| Towing speed [m/s] | Orientation [°] | Vibration frequency [rad/s] |
|---|---|---|
| 0.12 | 0 | 7.3631 |
| 0.24 | 0 | 16.8738 |
| 0.26 | 0 | 16.8738 |
| 0.26 | 30 | 17.4874 |
| 0.26 | 60 | 18.101 |
| 0.34 | 0 | 23.9301 |

The cross-flow natural frequencies and mode shapes of the catenary model were calculated in section 8. The results of the calculations showed that the effects of the bending stiffness on the eigenvalue problem were considerable. The results also suggest that the asymptotic expressions in equations (26) and (27) are good approximations to the cross-flow natural frequencies and mode shapes of the catenary model. Here we would like to compare the results of these asymptotic solutions to the measured dominant vibration frequencies in the cross-flow direction. First, the excited modes at the different towing speeds are identified by calculating the reduced velocities as:

$$U_r = \frac{U_{tow}}{f \cdot D} \qquad (33)$$

where $U_r$ is the reduced velocity, $U_{tow}$ is the towing speed, $f$ is the natural frequency in Hertz calculated from equation (27) and $D$ is the external diameter of the catenary model. Table 6 shows the calculated reduced velocities at the different towing speeds for the first ten modes.

Table 6: Reduced velocities at the different towing speeds for the first ten modes.

| **Mode #** | **Towing speed [m/s]** | | | |
|---|---|---|---|---|
| | **0.12** | **0.24** | **0.26** | **0.34** |
| **1** | 36.78 | 73.16 | 78.41 | 103.64 |
| **2** | 15.00 | 29.83 | 31.98 | 42.27 |
| **3** | **8.05** | 16.01 | 17.16 | 22.68 |
| **4** | 4.94 | 9.83 | 10.54 | 13.93 |
| **5** | 3.32 | **6.60** | **7.07** | 9.34 |
| **6** | 2.37 | 4.71 | 5.05 | **6.67** |
| **7** | 1.77 | 3.52 | 3.77 | 4.99 |
| **8** | 1.37 | 2.73 | 2.92 | 3.86 |
| **9** | 1.09 | 2.17 | 2.33 | 3.08 |
| **10** | 0.89 | 1.77 | 1.90 | 2.51 |

Lock-in is expected to occur at reduced velocities between 5 and 9. Based on the results in Table 6, the towing speed 0.12 and 0.34 m/s will excite the third and sixth modes, respectively. The fifth mode will be excited at towing speeds 0.24 and 0.26 m/s. Moe et al. [20] used the component of the flow velocity normal to the catenary axis $s$, when calculating the reduced velocity. This approach will not change the conclusions made here about the dominant excited modes. On the other hand, it would give some additional information about other excited modes. Figure 9 shows an example of the reduced velocities calculated using the normal velocity component when the catenary model was towed with a speed of 0.26 m/s at orientation of 0°.

Beside the dominant fifth mode, Figure 9 shows that the fourth mode could also be excited over a long portion of the catenary. The figure shows also that the lock-in occurs mainly in the upper part of the catenary suggesting that the upper end of the catenary will lead its lower end during the vibration and most likely there will be a phase difference along the catenary. Moe et al. [20] investigated the phase difference for this case and reported an estimated value of about 1 radian.

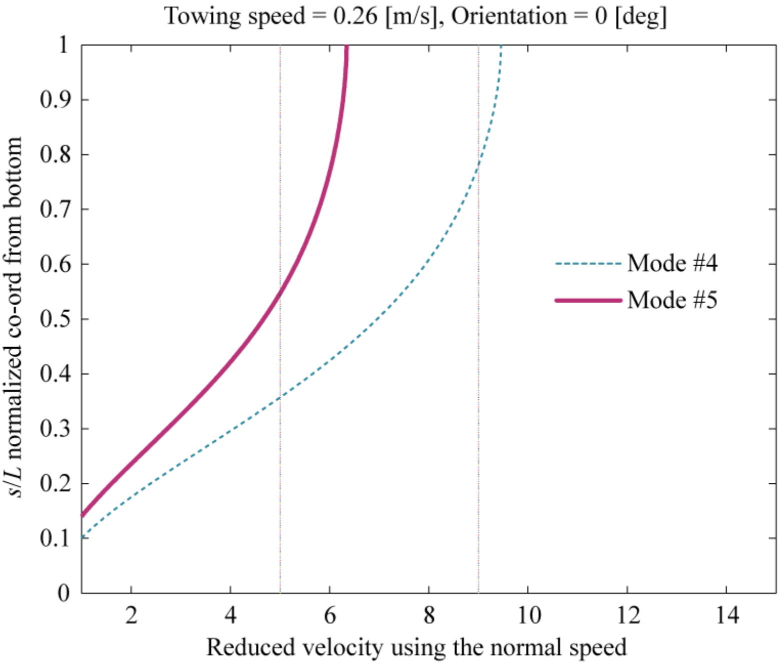

Figure 9: The reduced velocities along the catenary model based on the component of the velocity that is normal to the axis of the caternary.

Table 7 compares the natural frequencies calculated from equation (27) for the excited modes in the cross-flow direction to the measured dominant vibration frequencies.

Table 7: Comparison between the calculated and measured frequencies.

| Towing speed [m/s] | Orientation [º] | Excited dominant mode | Natural frequency [rad/s] | Vibration frequency [rad/s] | Percent error [%] |
|---|---|---|---|---|---|
| 0.12 | 0 | Third | 6.8132 | 7.3631 | -7.47 |
| 0.24 | 0 | Fifth | 16.5359 | 16.8738 | -2.00 |
| 0.26 | 0 | Fifth | 16.5359 | 16.8738 | -2.00 |
| 0.26 | 30 | Fifth | 16.5359 | 17.4874 | -5.44 |
| 0.26 | 60 | Fifth | 16.5359 | 18.101 | -8.65 |
| 0.34 | 0 | Sixth | 23.1659 | 23.9301 | -3.19 |

For all cases, the discrepancy between the calculated and measured frequencies was less than 10%. These results are promising and support the use of the asymptotic solutions. On the other hand, we must keep in mind that the error of the asymptotic solutions will decrease or increase depending on the added mass which has been set equal to the displaced mass herein, but is known to vary considerably, depending among other factors on the reduced velocity. For example, if the added mass is set arbitrarily equal to half of the displaced mass, the calculated natural frequencies will increase approximately 8.5%. The error of the asymptotic solutions will also be a function of the structural damping since the asymptotic solutions calculate only the un-damped natural frequencies. Moreover, it seems that the error increases by increasing the oblique angle of the flow direction. This could be expected because the assumption of decoupling the dynamics in the cross-flow and in-line directions becomes weaker at large angles. More cases, however, must be analyzed in order for this conclusion to be firm.

Figure 10 shows the envelopes of the measured motions of the catenary for the case of 0.26 m/s towing speed and 0° orientation angle. The left and right sides of Figure 10 are the motion envelops in the in-line and cross-flow directions, respectively. The envelopes are plotted based upon the maxima of the motions of the measuring points through which a curve was fitted by a spline routine. Previously, Figure 8 showed that the vibrations were dominated by a single frequency. In the framework of eigenvalue analysis, every frequency has a corresponding mode shape. Since the customary un-damped modal technique results in standing waves with nodes that exhibit zero motions, it is tempting to hypothesize that the VIV motion shown Figure 10 occur at a single complex mode in which the phase difference along the catenary is large, i.e. we are between standing and travelling waves. If that is the case, and we are trying to model this complex mode with real un-damped modes, then the shape would not fit. The travelling wave behavior (i.e. the complex mode shape) would give significant amplitudes also at what for the standing wave (un-damped mode shape) is a node. This spatial shape could be fitted as a combination of the 3 first un-damped mode shapes, however that is not entirely correct, since the complex mode will occur at a single natural frequency, while the 3 first un-damped mode shapes occur at different frequencies.

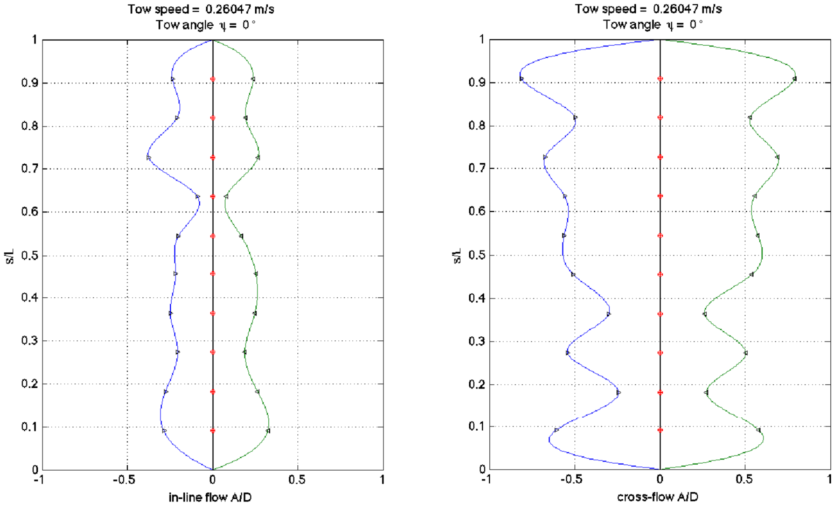

Figure 10: Measured motion envelopes of the experimental catenary model for the case of 0.26 m/s towing speed and 0° orientation angle.

Moreover, the envelope from the experiment consists of the most extreme occurrences at all point considered. In all likelihood they will occur at different times at different points, and may represent occasional odd behavior, especially at points that normally have moderate motions, i.e. are close to what are normally nodes in the mode shapes. On the other hand, mode shapes with amplitudes derived from the spectra are very much a manifestation of average behavior. From the measured time series (see Figure 7) we know that the difference between average behavior and extremes is large.

From the above discussion, it is evident that the use of the un-damped mode shapes solution to interpret the measurements and to reproduce the measured motion envelops is quite challenging. Some very interesting additional results could be obtained by a more in-depth analysis of the experimental data. This will require a substantial amount of work and will be left for continuation research paper.

## 10. Summary and Conclusions

This paper presents closed form asymptotic solutions of the cross-flow free vibrations of catenary cables and beams. The derivation of the solutions is based on the assumption that the dynamics of the catenary in the cross-flow direction is uncoupled from those in the in-line direction. The effects of bending stiffness on the static configuration of the catenary and on the natural frequencies and mode shapes are discussed. The effects of approximating the tension variation along the catenary by a linear function are also investigated. A finite element solution is presented and an in-house Matlab program based on that solution is used to verify the asymptotic expressions. Finally, the usefulness of the asymptotic solutions in predicting the dominant VIV frequencies is tested by comparing the calculated natural frequencies with data from an SCR model test program. The following list shows the conclusions from the present study:

- A catenary slender structure can be modeled either as a string or as a beam. When the dimensionless parameter $\lambda$, equation (32), is less than 1, the bending stiffness dominates and the cross-flow natural frequencies and mode shapes must be calculated using the beam model.

- For the string case, the asymptotic solutions which approximate the tension by a linear function yield quite satisfactory results for the cross-flow natural frequencies and mode shapes (relative difference is approximately 4%). On the other hand, the asymptotic solutions derived in this paper which account for the non-linear variation of the tension has improved the accuracy of the solutions (relative difference varies from about 1% in the first mode to 0.01% in the tenth mode). The second order asymptotic solution improved the prediction of the mode shapes compared to the first order solution but it had a little effect on the natural frequencies.

- For the beam case, equations (26) and (27) give quite good results for the cross-flow natural frequencies and mode shapes compared with the solutions that consider the non-linear tension variation along the catenary.

- For the experimental catenary model, the effects of bending stiffness were significant and therefore the beam model ought to be used to estimate the static configuration and also to estimate the cross-flow natural frequencies and mode shapes.

- The experimental data show that the catenary model was vibrating due to the vortex shedding with only small number of frequencies and usually the vortex induced vibration was dominated by a single frequency.

- In the six experimental cases presented in this paper, the discrepancy between the measured vibrations frequencies and those calculated from equation (27) was less than 10%. These results are promising and it promotes the use of the presented asymptotic solutions.

- More in-depth analysis of the experimental data is required in order to study the relationship between the measured envelops of motion and the calculated un-damped mode shapes.

## Acknowledgements

We would like to thank the STRDE project by 2H Offshore Eng. for granting access to the riser experiment. Thanks also goes to Mr. Halvor Lie at MARINTEK for his help in transferring and documenting the measured data and interpreting them.

## References

[1] Bliek, A., 1984, "Dynamic analysis of single span cables," Ph.D. thesis, Ocean Engineering Department, MIT.

[2] Kim, Y. C., 1983, "Nonlinear vibrations of long, slender beams," Ph.D. thesis, Ocean Engineering Department, MIT.

[3] Irvine, H. M., and Caughey, T. K., 1974, "The linear theory of free vibrations of a suspended cable," Proceedings of the Royal Society of London, Series A (Mathematical and Physical Sciences), Great Britain, Vol. 341, No. 1626, pp. 299-315.

[4] Triantafyllou, M. S., and Bliek, A., 1983, "The dynamics of inclined taut and slack marine cables," Proceedings of the 15th annual Offshore Technology Conference (OTC), Houston, Texas, Vol. 1, pp. 469-476.

[5] Triantafyllou, M. S., Bliek, A., and Shin, H., 1985, "Dynamic analysis as a Tool for open-sea mooring system design," Transactions of the Society of Naval Architects and Marine Engineers (SNAME), New York, Vol. 93, pp. 303-324.

[6] Moe, G., and Chucheepsakul, S., 1988, "The effect of internal flow on marine risers," Proceedings of the 7th International conference on Offshore Mechanics and Arctic Engineering (OMAE), Houston, Texas, pp. 375-382.

[7] Strømsem, K. C., 1989, "Dynamic Behavior of riser systems exposed to internal fluid flow – an analytical approach," Ph.D. thesis, Division of Structural Engineering, NTH.

[8] Lubbad, R. K., and Moe, G., 2008, "Closed-form solutions for vibrations of nearly vertical strings and beams by means of asymptotic methods," Journal of Engineering Mechanics, **134**(12), pp. 1064-1070.

[9] Chaplin, J. R., Bearman, P. W., Cheng, Y., Fontaine, E., Graham, J. M. R., Herfjord, K., Huera Huarte, F. J., Isherwood, M., Lambrakos, K., Larsen, C. M., Meneghini, J. R., Moe G., Pattenden, R. J., Triantafyllou, M. S., and Willden, R. H. J., 2005, "Blind

predictions of laboratory measurements of vortex-induced vibrations of a tension riser," Journal of Fluids and Structures, **21**(1), pp. 25-40.

[10] Moe, G., and Arntsen, O., 2001, "An analytic model for static analysis of catenary risers," Proceedings of the 11th International Offshore and Polar Engineering Conference (ISOPE), Stavanger, Norway, Vol. 2, pp. 248-253.

[11] Sparks, C. P., 2007, "Fundamentals of marine riser mechanics: basic principles and simplified analyses," PennWell Corporation: Tulsa, Oklahoma, USA, pp. 248-251.

[12] Bender, C. M., and Orszag, S. A., 1978, "Advanced mathematical methods for scientists and engineers," McGraw Hill: Signapore, pp.79

[13] Pesce, C. P., Fujarra, A. L. C., Simos, A. N., and Tannuri, E. A., 1999, "Analytical and closed form solutions for deep water riser-like eigenvalue problem," Proceedings of the 9th International Offshore and Polar Engineering Conference (ISOPE), Brest, France, Vol. 2, pp. 255-264.

[14] Cheng, Y., Vandiver, J. K., and Moe, G., 2002, "The linear vibration analysis of marine risers using the WKB-based dynamic stiffness method," Journal of Sound and Vibration, **251**(4), pp. 750-760.

[15] Kwon, Y. W., and Bang, H., 2000, "The finite element method using Matlab (Second edition)," CRC Press LLC: Florida, USA.

[16] Moe, G., Cheng, Y., and Vandiver, J. K., 2000, "Riser analysis by means of some finite element approaches," Proceedings of ETCE/OMAE2000 Joint Conference, New Orleans, LA, USA, pp. 141-146.

[17] Meirovitch, L., 1997, "*Principles and Techniques of Vibrations*," Prentice Hall

[18] Moe, G., and Hoen, C., 1999, "Dynamics of marine risers in term of complex eigenmodes," *Third International Symposium on Cable Dynamics*, Trondheim, Norway.

[19] Lie, H., 2001, "VIV Model of a Catenary Riser – STRIDE Ph.4," Technical Report No.512345.00.01, Norwegian Marine Technology Research Institute, Trondheim, Norway. (Confidential)

[20] Moe, G., Teigen, T., Simantrias, P., Willis, N., and Lie, H., 2004, "Predictions and model tests of an SCR undergoing VIV in flow at oblique angles," OMAE2004-51563, Proceedings of the 23rd international conference on Offshore Mechanics and Arctic Engineering (OMAE), Vancouver, British Columbia, Canada, pp. 1023-1034.

[21] Niedzwecki, J. M., and Moe, G., 2005, "Investigation of a catenary riser undergoing VIV," Fluid-Structure Interactions, La Coruna, Spain, Vol. 84, pp. 217-224.

[22] Niedzwecki, J. M., and Moe, G., 2007 "Development of SCR VIV in a Changing Flow Field," Fluid-Structure Interaction, New Forest, UK, Vol. 92, pp. 85-94.

# CHAPTER 5

## Experimental Investigations of the Efficiency of Round-Sectioned Helical Strakes in Suppressing Vortex Induced Vibrations

Is not included due to copyright

# CHAPTER 6

# A numerical model for real-time simulation of ship–ice interaction

Is not included due to copyright

# CHAPTER 7

# Static and Dynamic Interaction of Floating Wedge-Shaped Ice Beams and Sloping Structures

**$19^{th}$ IAHR International Symposium on Ice**
"Using New Technology to Understand Water-Ice Interaction"
*Vancouver, British Columbia, Canada, July 6 to 11, 2008*

# Static and Dynamic Interaction of Floating Wedge-Shaped Ice Beams and Sloping Structures

**Raed Lubbad, Geir Moe and Sveinung Løset**
*The Norwegian University of Science and Technology (NTNU)*
*Høgskoleringen 7A, 7491 Trondheim, Norway*
*Raed.lubbad@ntnu.no, geir.moe@ntnu.no, sveinung.loset@ntnu.no*

## Abstract

When level ice interacts with a sloping structure, or when a ship advances in level ice, the ice sheet may begin to fail by forming cracks in the radial direction. These radial cracks will be lengthened and increased in number until a circumferential crack is formed and consequently the ice sheet reaches its ultimate capacity. After the formation of the radial cracks the ice sheet can no longer be modelled as a continuum, instead it is common to use the model of adjacent wedges. This paper reviews the state-of-the-art in modelling the ultimate failure of an ice sheet using the model of adjacent wedge-shaped beams.

In this paper, both the static and dynamic problems are formulated for a floating wedge-shaped beam interacting with a sloping structure. For the dynamic interaction, the results of the elastohydrodynamic approach are compared with the model of Winkler foundation combined with added mass and hydrodynamic damping. The comparison shows that the elastohydrodynamic model is more reliable than the Winkler approach. The breaking lengths of the ice wedges are also investigated and it is concluded that the breaking lengths increase with increasing ice thickness and/or axial compression in the ice; while increasing the drift acceleration will always decrease the breaking lengths. The static results match the results of the elastohydrodynamic solution for small ice drift accelerations. The calculations are performed using the commercial finite element program "Comsol Multiphysics".

## 1. Introduction

Accurate predictions of ice actions are vital in order to optimise the design of structures in the Arctic regions. A good understanding of the ice-structure interaction process will help establishing reliable models to estimate the ice forces. When level ice drifts against a fixed structure, or when a ship advances in level ice, the ice forces will increase until the ice sheet fails and hence the forces exerted on the structure drop. The failure of the ice sheet may occur in different modes, namely crushing, bending, buckling or mixed mode where two or more of the failure modes are active at the same time. The ice properties, the structure width and the relative drift velocity control the mode of failure of the ice sheet. In the case of an ice sheet is being pushed at moderate speeds against a sloping structure, the bending failure of the ice sheet will dominate over the other modes of failure. Based on this hypothesis, the theory of an elastic plate resting on an elastic foundation "Winkler foundation" has been used to model the interaction between level ice and sloping structures. It is important at this point to highlight the influence of the relative drift velocity on the accuracy of the above mentioned model. A relatively low velocity between the ice and structure causes the behaviour of the ice to be inelastic rather than elastic. High speed interaction will make the accuracy of the Winkler foundation model questionable, since such foundations account only for the restoring forces from the water.

Hertz (1884) was the first to solve the static problem of an infinite floating plate with a vertical concentrated load at its origin in terms of infinite series. Later, Hetenyi (1946) and Wyman (1950) presented solutions to the same problem in terms of Bessel functions. The semi-infinite plate on elastic foundation with a vertical static load at the free edge was solved by Nevel (1965) and Kerr and Kwak (1993). All the aforementioned solutions which treat ice as a continuum are useful to predict the initiation of cracks in ice simply by comparing the stress in the ice sheet with a failure criterion, i.e. here the flexural strength of ice. On the other hand, these solutions can not predict the number and the extent of the cracks and hence they fail to estimate the ultimate failure of the ice sheet. One promising approach to overcome the limitation of the elastic plate theory is to implement the fracture mechanics concepts where the energy input from the external load is balanced by the energy dissipated in deforming the ice and creating the cracks. Recently fracture mechanics approaches have been used by several researchers to study the cracks initiation and propagation in ice. Nevertheless the state-of-the-art in studying the ultimate failure of an ice sheet is still based on the observations from experiments and full-scale, which suggest predefining the cracking patterns into radial and circumferential cracks. According to these observations, the ice begins to fail by forming cracks in the radial direction starting from the contact point. These radial cracks are due to the tension at the bottom of the ice plate. Increasing the forces applied on the ice will increase the number of the radial cracks and lengthen them until a circumferential crack is formed, see Nevel (1972).

The continuum approach using the elastic plate theory will not be able to model the circumferential cracks because the plate is already broken by the radial cracks. In order to predict these circumferential cracks, Nevel (1958) proposed replacing the plate by adjacent wedge-shaped beams resting on an elastic foundation. The first static solution of a wedge beam on elastic foundation under a vertical load at the apex was presented by Hetenyi (1946) in terms of simple functions. The solution of Hetenyi, however, diverges near the apex which makes it useless for the problems of ice-structure interaction. Nevel (1961) published a power series solution for a wedge with vertical static distributed load and his solution converges over the whole domain. In addition to the vertical force, there exists horizontal force acting on the wedge. This horizontal force will modify the stress in the wedge and it may cause the wedge to fail in buckling. Nevel (1979) solved the static problem of a wedge beam with horizontal and vertical loads analytically. He presented the solution in integral forms and was able to study the bending and buckling failure of the ice wedge. Later Nevel (1992) simplified the integral solution and republished it in terms of infinite series. In his new solution, Nevel neglected the effects of the horizontal force on the bending of the ice wedge and considered it only when calculating the flexural stress. The results of the buckling analysis from Nevel were confirmed by a numerical analysis conducted by Sodhi (1979). Sodhi used the finite element method (FEM) and considered a radial stress field for the in-plan stresses in the ice sheet.

Kerr (1978) provided approximate expressions for the static buckling forces of a semi-infinite wedge on elastic foundation. Li and Bazant (1994) examined the use of beam theory to solve the ice wedge problem. They used the finite difference method (FDM) together with the plate theory and finally concluded that the results of beam theory are sufficiently accurate for wedge angles up to $\pi/4$. Määttänen and Hoikkanen (1990) used the FEM to solve the static problem of wedge-shaped beam subjected to axial compression and distributed transverse load by discretizing the beam into finite elements and assuming a constant axial load along each element. McKenna and Spencer (1993) adopted the theory of beams on Winkler foundation to study the dynamics of the ice wedge using the FEM. They derived the mass and stiffness matrices for a wedge-shaped beam element and they assumed constant added mass and hydrodynamic drag coefficients when solving the dynamic equation of motion. Dempsey and Zhao (1993) investigated the validity of using added mass together with Winkler foundation for solving the dynamic problems of a floating ice sheet and they concluded that this approach can not model the dynamic response accurately because the added mass varies with time and space. Dempsey et al. (1999) presented an elastohydrodynamic approach to study the dynamic problem of floating ice beams where the ice is modelled as an elastic beam and the water is modelled as a potential flow. This paper studies the static and dynamic interaction between sloping structures and floating wedge-shaped ice beams. First the problem of dynamic interaction is formulated according to the elastohydrodynamic model. Second the model of Winkler foundation combined with added mass and hydrodynamic damping is discussed and finally the static problem is presented. The commercial finite element program “Comsol Multiphysics” is used to solve the interaction problem. The results are shown, discussed and finally conclusions are drawn.

## 2. Model Description

Figure 1 shows a wedge-shaped ice beam of thickness, $h$, and angle, $\theta$, floating on water of constant depth, $d$, and drifting against an upward sloping structure with slope angle, $\alpha$.

*a) Elastohydrodynamic model*

According to the elastohydrodynamic model, the governing differential equation of the floating wedge in Figure 1 is

$$\rho_i h \frac{d^2 w}{dt^2} + \frac{1}{b}\frac{d^2}{dx^2}\left[ E I \frac{d^2 w}{dx^2} \right] + \frac{H(t)}{b}\frac{d^2 w}{dx^2} - p_i(x,t) = q(x,t) \qquad (w = 0 \quad \text{at } t = 0) \qquad [1]$$

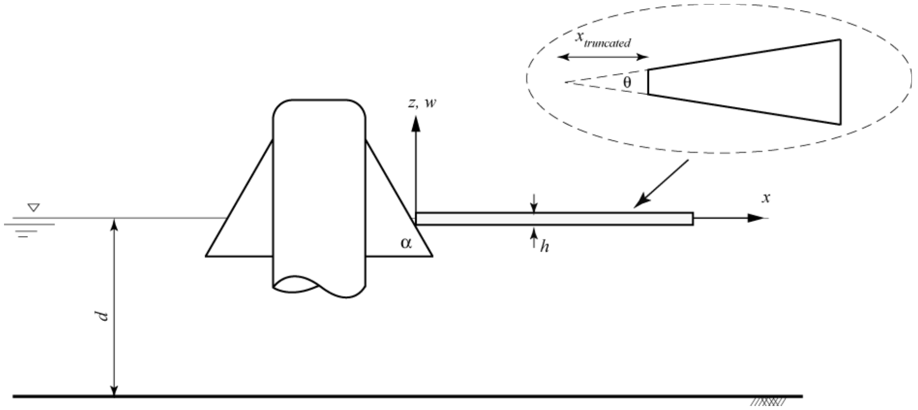

Figure 1. A floating ice wedge drifts against an upward sloping structure.

where $w$ is the transverse deflection of the beam, $x$ is the space coordinate along the beam, $t$ is the time, $\rho_i$ is the density of ice, $E$ is the modulus of elasticity, $I$ is the moment of inertia $\left(I = b \cdot h^3/12\right)$, $b$ is the width of the beam $\left(b = b_0 \cdot x\right)$, $b_0$ is the width of the beam at 1 m from the apex (Note: the wedge in this paper is truncated and so the width at $x = 0$ is $b_0 \cdot x_{truncated}$), $H$ is the in-plane compressive force, $p_i$ is the pressure on the bottom surface of the wedge due to the hydrodynamic reaction from the water and $q$ is the external applied pressure.

The wedge-shaped ice beam is surrounded by adjacent wedges and together they may still behave similar to a continuous ice cover. This means that the flow under the ice may well be assumed independent of the lateral direction and so a two-dimensional description for the hydrodynamic problem becomes justified. Assuming irrotational flow, the motion of the water is governed by potential theory where the velocity vector is expressed as the gradient of the velocity potential, $\phi(x,z,t)$, see Nevel (1970) and Fox and Chung (2002). The irrotational flow is also continuous (the water is incompressible) which means that Laplace equation must be satisfied in the water domain

$$\nabla^2\phi = \frac{\partial^2\phi}{\partial x^2} + \frac{\partial^2\phi}{\partial z^2} = 0 \qquad -d < z < 0 \qquad -\infty < x < \infty \qquad [2]$$

Equation 2 is a second order partial differential equation that has the following boundary conditions:

$$\frac{\partial\phi}{\partial z} = 0 \qquad z = -d, \qquad -\infty < x < \infty \qquad \text{(at the sea bed)}$$
$$\frac{\partial\phi}{\partial z} = \frac{\partial w}{\partial t} \qquad z = 0, \qquad 0 < x < \infty \qquad \text{(at the ice-water interface)}$$
$$\frac{\partial^2\phi}{\partial t^2} + g\frac{\partial\phi}{\partial z} = 0 \qquad z = 0, \qquad -\infty < x < 0 \qquad \text{(at the water free surface)} \qquad [3]$$

$$p_i + \rho_w g w + \rho_w \frac{\partial \phi}{\partial t} = 0 \qquad z = 0 \qquad -\infty < x < \infty \qquad \text{(linearized Bernoulli equation)}$$

$$\phi = 0 \qquad -d < z < 0, \qquad x = \pm\infty$$

where $\rho_w$ is the density of water and $g$ is the acceleration of gravity. If the ice sheet is drifting with a constant acceleration, $a$, against the sloping structure, the transverse deflection of the wedge at the contact point will be

$$w(0,t) = 0.5 \cdot a \cdot t^2 \cdot \tan(\alpha) \tag{4}$$

Solving equation 1 and 2 simultaneously and satisfying their boundary conditions in 3 and 4 will couple the physics of the elastic beam with that of the hydrodynamic foundation and this elastohydrodynamic solution is hoped to predict accurately the dynamic response of the floating beam. Here it is important to mention that the deflection of the ice before the breakup is typically much less than the ice thickness and therefore the partial emergence of the ice sheet prior the fracture is not considered in the present model.

*b) Dynamic model using Winkler foundation and added mass*

Several researchers used the model of elastic beam on Winkler foundation combined with added mass and hydrodynamic damping in order to study the dynamics of floating ice. In this case, equation 1 is replaced by

$$\rho_i h(1+c_a)\frac{d^2 w}{dt^2} + \rho_w c_w \left|\frac{dw}{dt}\right| \frac{dw}{dt} + \frac{1}{b}\frac{d^2}{dx^2}\left[E I \frac{d^2 w}{dx^2}\right] + \frac{H(t)}{b}\frac{d^2 w}{dx^2} + \rho_w g w = q(x,t) \tag{5}$$

where $c_a$ and $c_w$ are the added mass and hydrodynamic damping coefficients, respectively. Here, the hydrodynamic damping is mainly due to the viscosity in the boundary layer and therefore a linear damping term would be appropriate. However, a quadratic term is used in equation 5 following the presentation of McKenna and Spencer (1993) and the influence of this on the numerical results was found to be minor. The boundary conditions of equation 5 are the same as those of equation 1 and the solving techniques are pretty much the same. However, solving Laplace equation is not needed here in order to calculate the pressure under the ice wedge.

*c) Static model*

For the static and/or quasi-static interaction, the inertia and damping effects diminish and the model can be simplified as shown in Figure 2.

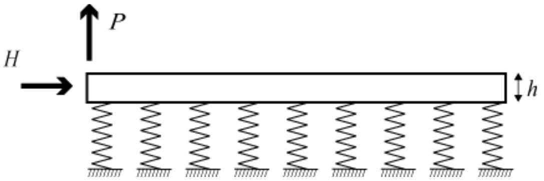

**Figure 2.** Wedge-shaped ice beam on elastic foundation (static interaction).

The governing differential equation becomes

$$\frac{1}{b}\frac{d^2}{dx^2}\left[E\,I\frac{d^2w}{dx^2}\right]+\frac{H(t)}{b}\frac{d^2w}{dx^2}+\rho_w\,g\,w=q(x,t) \qquad [6]$$

The static solution is not influenced by the rate of the deflection and therefore the boundary conditions can be applied simply as external static forces, i.e. $P$ is a vertical force and $H$ is a horizontal force, as shown in Figure 2.

In the following, the commercial finite element program "Comsol Multiphysics" is used in order to solve the static and dynamic problems of an ice wedge. Comsol Multiphysics solves the Euler-Bernoulli beam equation by modelling the ice wedge as plane stress where the Poisson's ratio is set equal to zero. Table 1 summarises the properties of this numerical model. In Table 1, the geometrical properties of the wedge and properties of the ice are chosen similar to those used by McKenna and Spencer (1993).

**Table 1.** The properties of the numerical model.

| | |
|---|---|
| Water free surface | $300\,\mathrm{m} \quad (-300 \le x < 0\,\mathrm{m})$ |
| Water depths $(d)$ | $120\,\mathrm{m} \quad (0 < z < 120\,\mathrm{m})$ |
| Wedge length $(L)$ | $300\,\mathrm{m} \quad (0 \le x \le 300\,\mathrm{m})$ |
| Wedge width at 1 m from the apex $(b_0)$ | 2.0 |
| Wedge truncated distance $(x_{\mathrm{truncated}})$ | $2.5\,\mathrm{m}$ |
| Wedge thicknesses $(h)$ | (0.3, 1.0) m |
| Ice flexural strength | $500\,\mathrm{kPa}$ |
| Ice modulus of elasticity $(E)$ | $3.5\,\mathrm{GPa}$ |
| Ice density $(\rho_i)$ | $900\,\mathrm{kg/m^3}$ |
| water density $(\rho_w)$ | $1025\,\mathrm{kg/m^3}$ |
| Structure slope from the horizontal $(\alpha)$ | $60^o$ |
| Drift accelerations $(a)$ | (0.001, 0.01, 0.1, 0.5, 0.7, 1.0) $\mathrm{m/s^2}$ |
| Added mass coefficient for Winkler-dynamic model $(c_a)$ | 1.23 |
| Hydrodynamic damping coefficient for Winkler-dynamic model $(c_w)$ | 1.0 |
| Structural damping | No structural damping |
| Solver type | Implicit |
| Wedge boundary conditions | Prescribed displacement at $x = 0\,\mathrm{m}$<br>(*For the static case: Loaded free edge at* $x = 0\,\mathrm{m}$)<br>Fixed at $x = 300\,\mathrm{m}$ |

## 3. Results and Discussion

Figure 3 shows the hydrodynamic reaction forces under the ice wedge at two different drift accelerations namely 0.001 and 0.5 m/s$^2$. The wedge thickness is 1 m and the hydrodynamic reaction forces are calculated using the elastohydrodynamic and the Winkler-dynamic models.

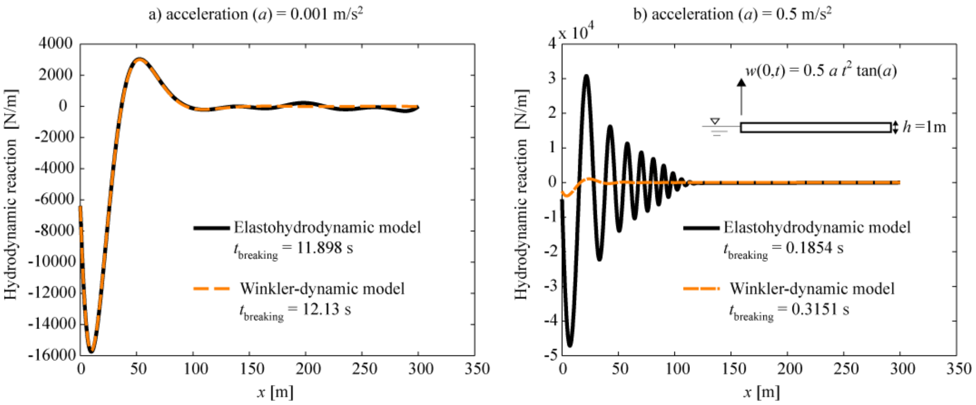

**Figure 3.** The hydrodynamic reaction forces at the breakup under the 1 m thick ice wedge drifting with the constant accelerations a) 0.001 and b) 0.5 m/s$^2$ (the results are according to the elastohydrodynamic and to the Winkler-dynamic models).

From Figure 3 it is evident that the results of the elastohydrodynamic and the Winkler-dynamic models are very similar at small drift accelerations. However, they diverge considerably at high accelerations. Figure 4 presents the flexural stress at the breakup for the same wedge discussed above. From the figure one sees that the elastohydrodynamic solution reaches the fracture slightly faster than the Winkler foundation solution. The breaking length of the wedge measured from the sloping structure is 7.76 m at small acceleration (0.001 m/s$^2$). At high acceleration (0.5 m/s$^2$), the breaking length is 4.5 m according to the elastohydrodynamic solution and 6.26 m according to the Winkler approach.

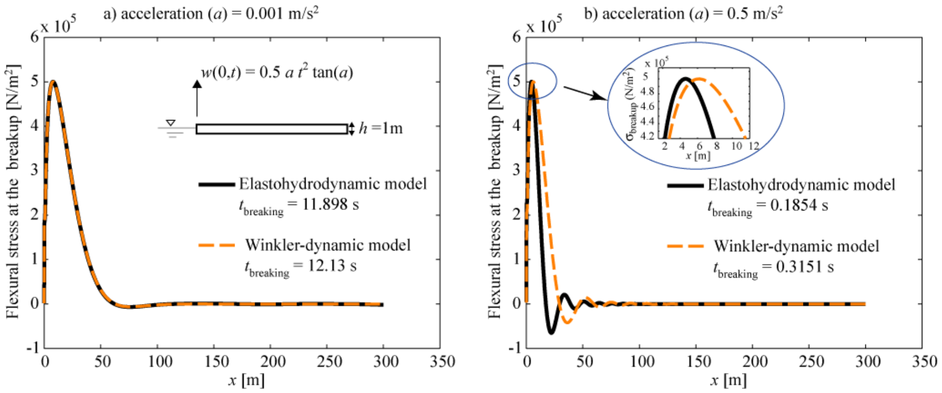

**Figure 4.** The flexural stress at the breakup of the 1 m thick ice wedge drifting with the constant accelerations a) 0.001 and b) 0.5 m/s$^2$ (the results are according to the elastohydrodynamic and to the Winkler-dynamic models).

The results of the Winkler model presented in Figures 3 and 4 may differ quite much if other values of the added mass were used. The Winkler-dynamic model could be improved by using an added mass coefficient that varies as a function of the wedge width. But such model will still be unable to consider the time variation of the added mass. All this indicates that the elastohydrodynamic approach is more reliable and the results obtained using Winkler foundation and added mass should be treated with some caution.

In order to investigate more closely the effects of drift acceleration on the breaking lengths of the above wedge, the elastohydrodynamic approach is used and the accelerations are varied from 0.001 to 1.0 m/s$^2$. The results of the flexural stress at the breakup are illustrated in Figure 5 and they show clearly that the breaking lengths reduce as the drift acceleration increases.

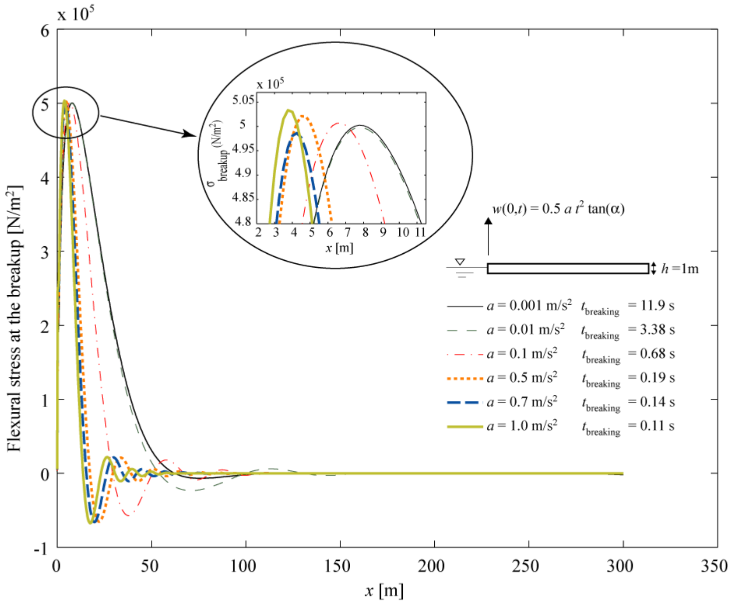

**Figure 5.** The flexural stress at the breakup of the 1 m thick ice wedge drifting with the constant accelerations 0.001, 0.01, 0.1, 0.5, 0.7 and 1.0 m/s$^2$ (the results are according to the elastohydrodynamic).

After subsequent breaking of ice, rubbles are created and typically accumulated in front of the sloping structures. The rubble accumulation causes the ice wedges to push through the rubbles during the interaction with the structure. As a result, the wedge will be subjected to axial compression from the rubble in addition to the horizontal and vertical forces from the structure. The effect of this axial compression on the breaking lengths of the wedge is examined in this paper. An axial force of 22.5 MN is used as an example and the results of the breaking lengths as a function of the drift acceleration are shown in Figure 6. Note that emphases are placed on the bending failure and any other possible modes of failure e.g. crushing are ignored here.

Figure 6 highlights also the effects of ice thickness on the breaking lengths by presenting the breaking lengths of a 30 cm thick wedge as a function of the drift accelerations. The information obtained from Figure 6 suggests that increasing the ice thickness and/or the axial compression in ice will increase the breaking lengths; in the mean time increasing the drift acceleration will always decrease the breaking lengths.

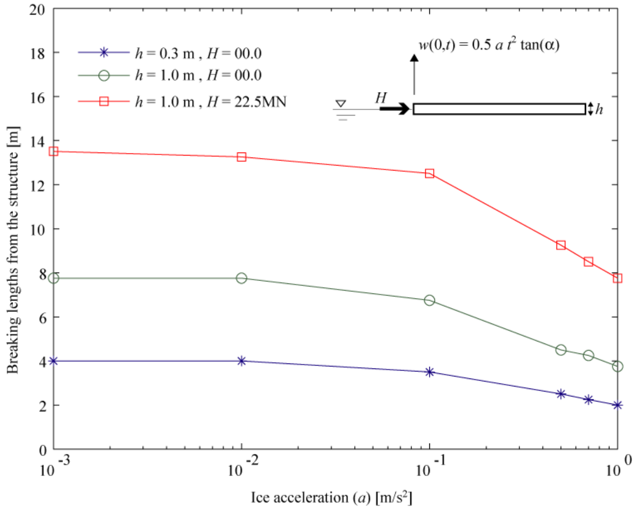

**Figure 6.** The breaking lengths of several wedges as a function of the ice drift accelerations.

Figure 7 shows the results of the static analysis. The analysis included three wedges. The first is 0.3 m thick, the second is 1 m thick and the third is 1 m thick and subjected to axial force of 22.5MN. The vertical static forces that caused failure in these wedges are 33.36 kN, 261.7 kN and 320.2 kN, respectively. The breaking lengths are 4.0 m, 7.76 m and 13.51 m, respectively. Here, it is interesting to note that these static breaking lengths match well with the dynamic breaking lengths calculated from the elastohydrodynamic model for small drift accelerations.

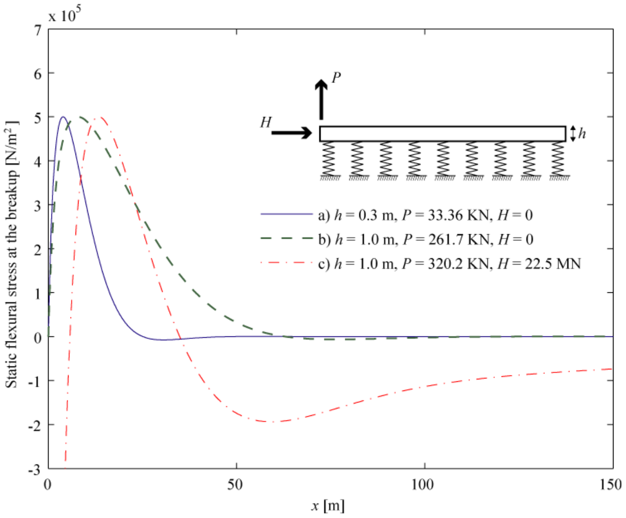

**Figure 7.** The static flexural stress of several wedges.

## 4. Conclusions

This paper looked at the static and dynamic interaction of floating wedge-shaped ice beams and sloping structures. The ice is assumed to fail only in bending and any transition in the failure mode is not considered. The most important finding are summarised as follows

- The elastohydrodynamic approach is reliable when modelling the dynamic interaction of ice wedge and sloping structures.
- The Finite Element Method provides a powerful tool to solve such elastohydrodynamic model.
- The results obtained using Winkler foundation and added mass should be treated with some caution.
- The breaking lengths increase by increasing the ice thickness and/or the axial compression in ice; meanwhile increasing the drift acceleration will always decrease the breaking lengths.
- The static solution matches well with the elastohydrodynamic solution at small ice drifts accelerations.

A thorough parametric study is needed in order to understand more the influence of the different parameters on the interaction process. In addition to the parameters introduced in this paper, several other parameters should also be included in the study such as the water depth, constant drift velocities, vertical distributed loads, and the area of the distributed load …etc.

## 5. References

Dempsey, J.P. and Zhao, Z.G., 1993. Elastohydrodynamic response of an ice sheet to forced sub-surface uplift. Journal of the Mechanics and Physics of Solids, Vol. 41, No. 3, pp. 487-506.

Dempsey, J.P. and Fox, C. and Palmer, A.C. 1999. Ice-slope interaction: Transitions in failure mode. Proceedings of OMAE, P&A-1156, St John’s, Newfoundland, Canada.

Fox, C. and Chung, H., 2002. Harmonic Deflections of an Infinite Floating Plate. Department of Mathematics Research reports Series, University of Auckland, No. 485, 33 p.

Hertz, H., 1884. Über das Gleichwicht schwimmender elastischer Platten. Annalen der Physik und Chemie, Vol. 22(7), pp. 449–455.

Hetenyi, M., 1946. Beams on elastic foundations. The University of Michigan Press, Ann Arbor, 255 p.

Kerr, A.D., 1978. On the determination of horizontal forces a floating ice plate exerts on structure. Journal of Glaciology, Vol. 20, No. 82, pp. 123-134.

Kerr, A. D. and Kwak, S. S., 1993. The semi-infinite plate on a Winkler base, free along the edge, and subjected to a vertical force. Archive of Applied Mechanics, Vol. 63, pp. 210-218.

Li, Y.N. and Bažantm Z.P. 1994. Penetration fracture of ice plate: 2D analysis and size effect. Journal of Engineering Mechanics, Vol. 120, No. 7, Jul, pp. 1481-1498.

Määttänen, M. and Hoikkanen, J. 1990. The effect of ice pile-up on the ice force of a conical structure. Proc. IAHR Ice Symposium, Espoo, Finland, Vol. 2, pp. 1010-1021.

McKenna, R.F. and Spencer, D. 1993. Ice wedge dynamics and local crushing. The 12th international conference on Port and Ocean Engineering under Arctic Conditions, Hamburg, pp. 85-96.

Nevel, D. E., 1958. The narrow infinite wedge on elastic foundation. Transactions of the Engineering Institute of Canada, Vol.2, No.3, pp. 132-140

Nevel, D. E., 1961. The narrow free infinite wedge on elastic foundation. CRREL Research Report 79, 24 p.

Nevel, D. E., 1965. Semi-infinite plate on elastic foundation. USA, CRREL Research Report 136, 14 p.

Nevel, D.A., 1970. Vibration of a floating ice sheet. CRREL Research report 281, Hanover, New Hampshire, 9 p.

Nevel, D. E., 1972. The ultimate failure of a floating ice sheet. International Association of Hydraulic Research (IAHR), Ice Symposium, Leningrad, pp. 17-22.

Nevel, D. E. (1979): Bending and buckling of a wedge on elastic foundation. IUTAM Ice Symposium, Physics and Mechanics of Ice, Copenhagen, pp. 278-288.

Nevel, D. E., 1992. Ice forces on cones from floes. Proc. 11th IAHR Symposium on Ice, Banff, Alberta, Vol. 3, pp. 1391-1404.

Sohdi, D.S., 1979. Buckling analysis of wedge-shaped floating ice sheets. Port and Ocean Engineering under Arctic Conditions Conference, Trondheim, Norway, pp. 797-810.

Wyman, M., 1950. Deflections of an infinite plate. Canadian Journal of Research, Vol. A28, pp. 293-302.

## CHAPTER 8

# SUMMARY, CONCLUSIONS AND RECOMMENDATIONS FOR FURTHER WORK

## Contents

**8. SUMMARY, CONCLUSIONS AND RECOMMENDATIONS FOR FURTHER WORK** ........ 109

**8.1 Summary and Conclusions** ........ 109

**8.2 Recommendations for further work** ........ **112**

# 8 SUMMARY, CONCLUSIONS AND RECOMMENDATIONS FOR FURTHER WORK

## 8.1 Summary and Conclusions

This thesis highlights some aspects related to the analyses of offshore structures. The thesis consists of five papers that can be divided into two main parts as follows.

*Part I: Dynamics of Slender Offshore Structures*

In the present work, two asymptotic techniques, namely, the local analysis and the WKB methods, are used to derive closed-form solutions for the natural frequencies and mode shapes of marine slender structures. Both the top-tensioned nearly-vertical configuration and the catenary configuration are considered in this study. The derived closed-form solutions are used to predict the susceptibility of marine slender structures to vortex induced vibrations (VIV). Additionally, the efficiency of round-sectioned helical strakes in suppressing the VIV of slender offshore structures is investigated in this thesis. The major conclusions are as follows.

*a) Dynamics of top-tensioned nearly-vertical slender structures*

- The vibrations of a tensioned string are analysed by means of an asymptotic technique called “local analysis.” Good approximations to the natural frequency may be found by a simple one-term asymptotic solution (Chapter 3: Eq. 22), while a two-term asymptotic expression (Chapter 3: Eq. 28) gives excellent approximate results.

- The vibrations of a beam with varying tension are analysed by the WKB method. The leading behaviour is described by an exponential function whose argument is an integral. Previously, this integral was solved numerically; however, in this thesis, a transformation is used so that a closed-form analytic expression is found. The same transformation also substantially simplifies the derivation of the next term in the WKB expansion. The solution (Chapter 3: Eq. 49) is in the form of exponential functions whose arguments are simple algebraic expressions. These expressions are in terms of elementary functions and are easily programmed, e.g., in Matlab. In the proposed formulation, they are also numerically stable. The example calculations show that the results are quite accurate.

- One attractive feature of asymptotic solutions is that the accuracy increases for higher mode numbers while conversely finite element methods need an increasing number of elements as the mode number increases. Thus, from the fourth mode onwards, both the string and the beam results in the example in Chapter 3 are accurate to four digits.

*b) Dynamics of catenary slender structures*

- A catenary slender structure can be modelled either as a string or as a beam. When the dimensionless parameter $\lambda$ (Chapter 4: Eq. 32) is less than 1, the bending stiffness dominates, and the cross-flow natural frequencies and mode shapes must be calculated using the beam model.

- For the string case, the asymptotic solutions, which approximate the tension as a linear function, yield quite satisfactory results for the cross-flow natural frequencies and mode shapes. On the other hand, the asymptotic solutions derived in this thesis, which account for the non-linear variation of the tension, improve the accuracy of the solutions. The second order asymptotic solution improves the prediction of the mode shapes compared to the first order solution, but it has a small effect on the natural frequencies.

- For the beam case, Eqs. 26 and 27 in Chapter 4 give quite good results for the cross-flow natural frequencies and mode shapes compared with the solutions that consider the non-linear tension variation along the catenary.

- The experimental data showed that the catenary model was vibrating due to the vortex shedding with only a small number of frequencies, and, usually, the vortex induced vibration was dominated by a single frequency.

- In the six experimental cases presented in this thesis, the discrepancy between the measured vibration frequencies and those calculated from Eq. 27 in Chapter 4 is less than 10%. These results are promising, and they support the use of the proposed asymptotic solutions.

c) *Efficiency of round-sectioned helical strakes in suppressing the VIV of slender structures*

- One-start round-sectioned helical strakes (helical strakes with only one rope) are not efficient in reducing VIV. This result is valid for all strake pitches and diameters tested. The simplest explanation for this finding is that one rope is insufficient to create three-dimensional flow over the whole length of the cylinder. This allows two-dimensional vortices to shed from different parts of the cylinder in a manner sufficient to permit VIV to build up.

- The main finding in this thesis concerning round-sectioned helical strakes is that the best configuration appears to be three starts, a $5D$ pitch and a $0.15D$ strake diameter. It reduces the amplitude of oscillation relative to the bare cylinder by 96% in the cross-flow direction and by 97% in the inline direction.

- The efficiency of the above-mentioned best round-sectioned helical strakes is not very sensitive to the pitch of the strakes. Nearly the same performance was obtained with pitches ranging from $3.5D$ to $8D$.

- Surface roughness may moderately reduce the efficiency of the selected configuration of round-sectioned helical strakes, as large grits have more influence on the VIV than small grits. However, the roughness did not change the trend of the vibration amplitudes in the lock-in range.

- The frequency ratio of the test cylinder affects the cylinder response. Within the range tested, low frequency ratios give higher amplitudes of oscillations, and high frequency ratios present wider lock-in ranges.

*Part II: Actions of Sea Ice on Floaters*

In this thesis, a numerical model is developed to simulate in real time the process of interaction between sea ice and floaters (e.g., conical structures and ship-shaped structures). Only level- and broken-ice features are considered. The present work also studies some aspects related to the dynamic interaction between ice and floaters. The thesis investigates the effects of the seawater on the dynamic bending problem of a floating wedge-shaped ice beam interacting with a sloping structure. The major conclusions can be summarised as follows:

*a) A numerical model for real-time simulation of ice-floater interactions*

- A numerical real-time simulator for ice-floater interactions has been developed. The theoretical foundation of the simulator is explained in detail in Chapter 6. The modelling of such a complex process of ice-floater interaction is very demanding and often computationally expensive, which typically hinders the chances for real-time simulations. This challenge is overcome in the present study, and the real-time criterion is achieved in the simulator, which is made possible for the following reasons.
    - The development of a new analytical closed-form solution of the maximum stress in a semi-infinite ice sheet resting on an elastic foundation and loaded with a vertical distributed load.
    - The use of the *PhysX* to solve the equations of rigid body motions in 6 DOF for all ice floes in the calculation domain.
- The results of the simulator are validated against the experimental data from model-scale and full-scale tests. The validation tests exhibited a satisfactory agreement between the simulator model calculations and the experimental measurements. Therefore, it is sound to conclude that the presented theoretical model, even with all its limitations, is able to produce results in real time that are quite accurate.
- Finally, the present real-time simulator has large potential in a number of applications. It can be used to train personnel for Arctic operations and procedures and to analyse the efficiency of different ice management concepts, and, in the future, such simulators may be a part of the onboard support systems for station keeping of Arctic offshore floaters.

*b) Aspects related to the dynamic interaction between level ice and floaters*

This thesis studies the static and dynamic interactions of floating wedge-shaped ice beams and sloping structures. The ice is assumed to fail only in bending, and any transition in the failure mode is ignored. The most important findings are summarised as follows:

- The fully coupled elasto-hydrodynamic approach makes it possible to study the effects of seawater (the water foundation) on the dynamic interaction of an ice wedge and a sloping structure.
- The results obtained using a Winkler foundation and added mass coefficient should be treated with some caution because the real added mass varies in time and space.

- The breaking lengths increase by increasing the ice thickness and/or the axial compression in ice. Meanwhile, increasing the drift acceleration will always decrease the breaking lengths.

- The static solution matches well with the elasto-hydrodynamic solution at small ice drifts accelerations.

## 8.2 Recommendations for further work

Based on the present study, the following topics can be suggested for further work:

- When analysing the experimental data obtained from the catenary model undergoing VIV, it seems that the deviation between the measured and calculated vibration frequencies increases by increasing the oblique angle of the flow direction to the catenary plane. This effect can be expected because the assumption of decoupling the dynamics in the cross-flow and in-line directions becomes weaker at large angles. More cases, however, must be analysed for this conclusion to be firm.

- More in-depth analysis of the experimental data of the catenary model undergoing VIV is required to study the relationship between the measured envelopes of motion and the calculated cross-flow undamped mode shapes.

- The efficiency of the suggested configuration of round-sectioned helical strakes still needs additional verification against the effects of 1) turbulence length scales, 2) critical and supercritical Reynolds numbers, and 3) low mass damping parameters of the test rig.

- Regarding the numerical model for the real-time simulation of ice-floater interactions, the relative significance of each process that contributes to the global ice resistance should be examined carefully in future research. Additionally, some attention should be given in future research to the processes that are not yet modelled in the simulator, e.g., the ventilation and the dependency of the breaking length on the speed.

- The results of the real-time simulator of the ice-floater interaction highlight the ability of the Newtonian dynamic calculations to synthesise the data, which agree with the experimental measurements. The ice forces calculated from the rigid body motion module dominate, and they are speed dependent, which provides a useful insight into the effects of speed on the interactions between the ice and, e.g., conical structures. The use of the present approach is highly recommended for further investigations into the modelling of the speed effects.

- When studying the dynamic interaction between wedge-shaped ice beams and sloping structures, the two-dimensional elasto-hydrodynamic model was useful to highlight the influence from the water foundation. The next step should be to upgrade the current model to a three-dimensional model.

- A thorough parametric study is needed to better understand the influence of the different parameters on the dynamic bending of a wedge-shaped ice beam. In addition to the parameters introduced in this thesis, several other parameters should also be included in the study, such as effect of the water depth, constant drift velocities, vertical distributed loads, and the area of the distributed load.